Article

Permian Granitic Plutons from the Northern Margin of the North China Craton: Implications for the Tectonic Evolution of the Central Asian Orogenic Belt

Jingsheng Chen [1,2], Dexin Tian [3], Bin Li [1,2,*], Yi Shi [4,*], Zhonghui Gao [5], Yi Tian [5], Weiwei Li [5], Chao Zhang [1,2] and Yan Wang [1,2]

1   Shenyang Geological Survey Center of China Geological Survey, Shenyang 110034, China; jschen0712@126.com (J.C.); congray@163.com (C.Z.); wangy68413@163.com (Y.W.)
2   Northeast Geological S&T Innovation Center of China Geological Survey, Shenyang 110034, China
3   Non-Ferrous Metals Geological Exploration Bureau of Zhejiang Province, Shaoxing 312000, China; tiandx12@mails.jlu.edu.cn
4   School of Resource & Environment and Safety Engineering, University of South China, Hengyang 421001, China
5   Institute of Geology and Mineral Resources of Liaoning Co., Ltd., Shenyang 110029, China; 13897938707@163.com (Z.G.); lnsytianyi@163.com (Y.T.); 15040028747@163.com (W.L.)
*   Correspondence: libin@mail.cgs.gov.cn (B.L.); aiwen9@126.com (Y.S.)

Abstract: As the world's largest accretionary orogen, the Central Asian Orogenic Belt (CAOB) underwent continuous juvenile crustal growth in the Phanerozoic. The northern margin of the North China Craton (NCC) and its adjacent area form the eastern segment of the CAOB, which is a key area for learning about the geological evolution of the Paleo-Asian Ocean (PAO). In the Permian, the west of the northern margin of the NCC was a post-collision extensional environment, while the east was in a subduction stage. As a connecting area, the Permian evolution of the PAO in the middle of the northern margin of the NCC has not been systematically studied. In order to fill the gap and understand the continuous temporal and spatial evolutionary process of the PAO, this paper focuses on the Permian granitic rocks in the Chifeng area. Zircon U-Pb dating and the geochemical analysis of whole-rock major and trace elements were conducted to build a granite chronological framework, and to discuss the genesis and tectonic background of the granitic rocks, along with tectono-magmatic evolutionary history in the Chifeng area. The respective LA-ICP-MS zircon U-Pb dating results from eight samples are 269 ± 1, 268 ± 3, 260 ± 4, 260 ± 1, 260 ± 1, 255 ± 2, 254 ± 2 and 256 ± 1 Ma, respectively. These results, combined with previous data, revealed that the Permian granitic rocks had undergone three events of magmatism: (1) monzogranitic-syenitic phase (294–284 Ma; Cisuralian); (2) monzogranitic phase (269–260 Ma; Guadalupian) and (3) late monzogranitic-syenitic phase (256–254 Ma; Lopingian). From the Early Permian (294–284 Ma) to the Middle Permian (269–260 Ma), granites with fine-medium-grained locally porphyritic texture and massive structure showed a high-potassium calc-alkaline series formed in a compressional setting, indicating a continuous collision between the Xing'an-Mongolian Orogenic Belt (XMOB) and the NCC. During the Late Permian-Early Triassic (256–248 Ma), granites with massive structure and medium-grained texture in the Chifeng area were magmatism dominated by A- and I-type granites of high-potassium calc-alkaline series, combined with the coeval basic rocks, which constituted a typical "bimodal" rock assemblage. This suggests that the Chifeng area was located in an extensional setting where the subducting slab broke off during the collision between the XMOB and NCC. These granitic plutons from the Permian are believed to have been generated by the subduction-collision of the Paleo-Asian oceanic crust beneath the NCC, according to emplacement time and occurrence location. Our findings provide strong evidence for Permian continuous temporal and spatial tectonic evolution and the characterization of the eventual closure of the PAO in Chifeng area at the northern margin of the NCC.

1. Introduction

As the world's largest Phanerozoic subduction-accretion orogen, the Central Asian Orogenic Belt (CAOB) is located between the Siberian Plate (SP) and the North China Craton (NCC). Its formation is closely related to the evolution of the Paleo-Asian Ocean (PAO) [1–3]. The CAOB adjacent to the northern margin of the NCC is also known as the Xing'an-Mongolian Orogenic Belt (XMOB), which is the orogenic belt with the longest evolutionary history and the most complicated tectonic and magmatic activities in China (Figure 1a). Its formation is related to the closure of the PAO, continental crust accretion, and extensive long-lasting tectonic–magmatic activities throughout the Phanerozoic [4,5]. As a result, the XMOB was formed by the accretion of microcontinents and Phanerozoic orogenic belts [6]. After intense continental growth and multi-stage geological evolution, the XMOB had a complex and diverse structure and crustal composition, being rich in oil and gas and metal mineral resources. Therefore, it has become a natural laboratory for scholars around the world to study continental dynamic evolution, magmatism, and ore metals [3].

The PAO has undergone a long and complex evolutionary history, as concluded from various investigations. As the mid-ocean ridge expanded and the ocean reached its maximum width, the oceanic crust began to subduct toward the continental margins on both sides. Then, the PAO basins contracted and eventually closed, leading to the collision and amalgamation of the micro-continents between the two major plates [7,8]. After the collision, it entered the post-orogenic stage of stress relaxation, and a series of complex continental crust transformation events began to occur, including extension, structural collapse, and lithosphere delamination [9–11]. Increasing data show that the Solonker-Xar Moron-Changchun-Yanji Suture (SXCYS) is the final location where the two major plates collided and joined [7,12–16]. Currently, the focus of debate is the time of collision and suturing, including the following four main points of view:

(1) Based on the analysis of sedimentary petrography, mixed accumulation of ophiolite, formation of stratigraphic deposition, and contact between the Carboniferous strata and ophiolite, it has been proposed that the northern margin of the NCC and the XMOB collided and collaged in the early Late Paleozoic, resulting in the complete subduction of the PAO [17,18]. Since the Late Carboniferous and after the SP and NCC were united through the XMOB, the study area has been characterized by intracontinental rifting magmatic and sedimentary activities [17,18]. It is believed that the Permian basin is a new rift basin with extension-related volcanic activities [17]. Some scholars also believe that the PAO closed before the Early Permian based on magmatism [19,20].

(2) Based on the study on the Early-Middle Permian alkaline granites in the northern margin of the NCC, is assumed that the time limit for the final merging of the northern margin of the NCC and the XMOB to be the Early-Middle Permian [10,13,21,22].

(3) Some scholars consider that the subduction of the PAO occurred in the Late Paleozoic, and its closure took place in Late Permian to Early Triassic times based on (I) paleomagnetism, mixing of paleontological groups, and biological extinction events suggesting that the PAO closed at the end of the Permian [2,23,24]. (II) Geochronological and geochemical data of magmatism show that a post-collision extensional environment can be interpreted for the Early Triassic. Therefore, the closure of the PAO was delimited as Late Permian [4,8,12,25–29]. (III) Oceanic Carboniferous basalts and Permian fossil content were discovered in the north of the Xar Moron River [30,31]. The reefs and marine fossils of the late Permian and the P/T unconformity surface exposed in Balin Right Banner, Inner Mongolia, and Jiutai County, Jilin, proved that the PAO closed at the end of the Late Permian [32]. (IV) Ophiolite suites obducted in

the Late Permian-Early Triassic in the island arc/back-arc environment, indicating the two plates likely collided in this period [7,33–36]. (V) The zircon U-Pb age of the Permian clastic deposits in Balin Left Banner showed the final collision and merged time of the two plates were likely later than 266 Ma [37].

(4) Other researchers believe that the collision between the the NCC and SP occurred at the end of the Late Permian and lasted for a long time until the Late Triassic, based on the Middle Permian-Middle Triassic syn-collision granite [28,38] and Late Triassic post-orogenic granite [8,16,29,31,39,40].
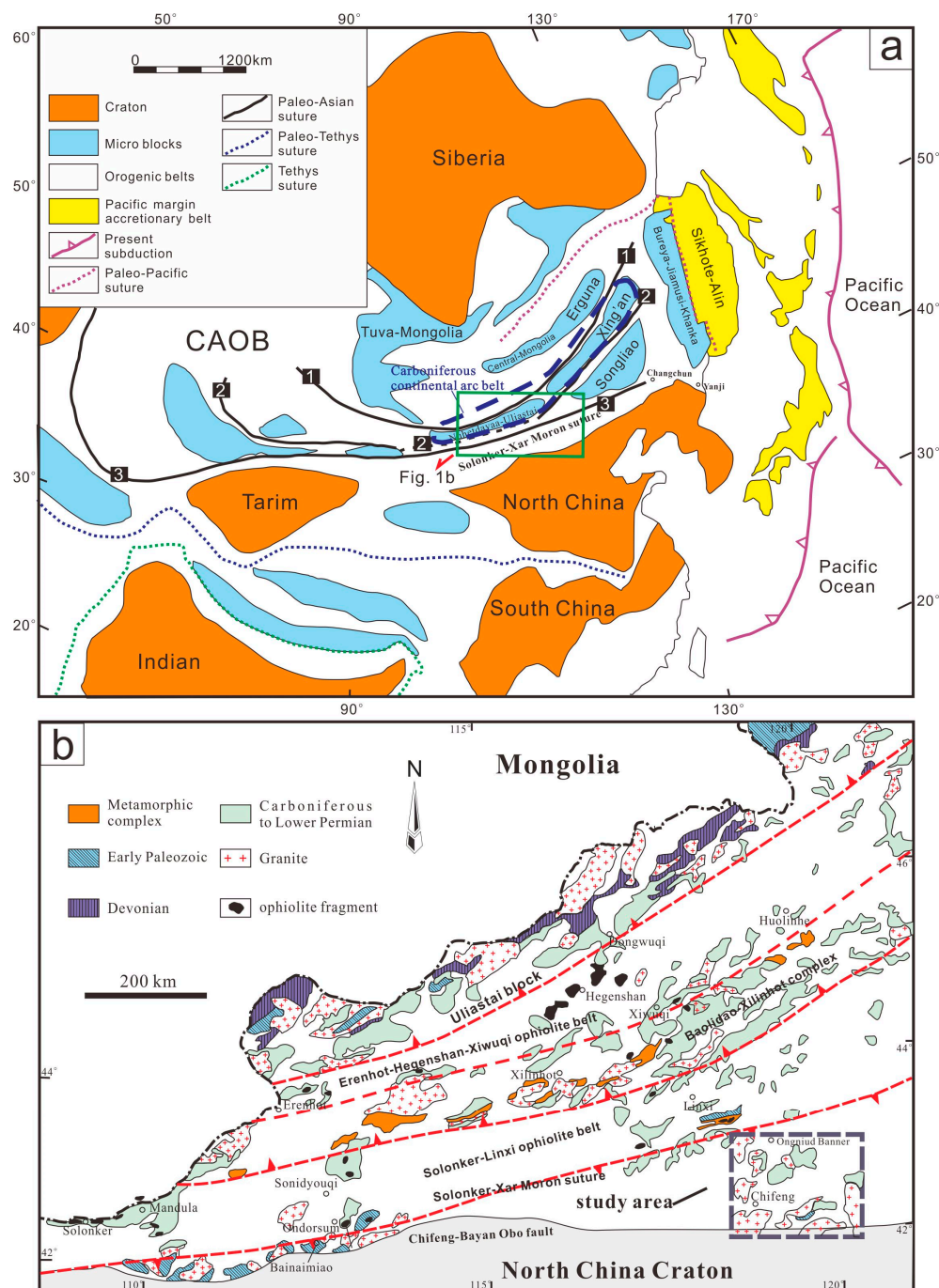

Figure 1. (**a**) Schematic tectonic map showing main tectonic subdivisions of central and eastern Asia and location of northeast China (modified from Li, 2006) [4]; (**b**) simplified geological map of central Inner Mongolia of the CAOB showing different tectonic units (modified from [7,8]).

The Chifeng area of Inner Mongolia, located at the junction of the XMOB and the northern margin of the NCC, is a key area to study the attributes, boundaries, collision and merging, and magmatic-tectonic evolution of the two tectonic units [17]. In recent years, geologists have identified multiple phases of granite assemblages from the Early Paleozoic to Mesozoic in southeastern Inner Mongolia: high-potassium, calc-alkaline series rock assemblages formed in an active continental margin environment [5,8,9,15,41,42]; potassium feldspar granites and monzogranite with syn-collision properties formed in a compressional environment [9,31,41]; and bimodal volcanic rocks and alkaline complex assemblages formed in a post-orogenic extensional environment [13,37,39]. These granites were formed in different magmatic-tectonic evolutionary stages during the PAO's closure and are controlled by different geodynamic backgrounds. Scholars have established the Triassic evolution model of the PAO by systematically studying the Triassic granitic rocks exposed in the Chifeng area [8]. However, the evolutionary process of the PAO in the Permian remains unclear. This study of the Permian granitic rocks exposed in the Chifeng area of the central-northern margin of the NCC, based on detailed field geological surveys, petrography, and geochemical and geochronological data, aims to shed light on the temporal and spatial tectonic–magmatic evolution of the PAO.

2. Geological Setting and Sample Descriptions

2.1. Geological Setting

The Chifeng area is located along the central-eastern part of the CAOB, between the Solonker-Xar Moron-Changchun-Yanji Suture (SXCYS) and Chifeng-Kaiyuan Fault (Figure 1b). Due to the quaternary covering, the bedrock mainly is composed of granitic rocks and the strata from different epochs [8,42]. The study area is bounded by the Chifeng-Kaiyuan Fault; the northern part belongs to the CAOB, showing Ordovician, Silurian, Carboniferous, and Permian strata (Figure 1b); and the southern part belongs to the NCC, showing Neoarchean metamorphic rocks and the Paleoproterozoic Baoyintu Group. During the Mesozoic, the Paleozoic basement was faulted, and the study area was transformed into an extensional basin. Continental molasse- and coal-bearing clastic rock formed in the early and Middle Jurassic; volcanic rocks formed in the Late Jurassic, and coal-bearing sediment was deposited in the Cretaceous. The graben basin formed in the Mesozoic era and changed over time due to uneven movements in the Cenozoic era. Sedimentary rocks were deposited in rivers and lakes, and basic volcanoes erupted [42].

2.2. Geological and Petrological Characteristics of Permian Granitoid Intrusions

There has been a lack of research on the granites in the Chifeng area. In recent years, in the process of regional geological surveys in Yuanbaoshan, Pingzhuang, Aohan Banner, and Beizifu in the east of Chifeng City, the author has disintegrated the plutons from 1:200,000 geological maps of Aohan Banner, Xiawa, and Chifeng City. Nine different Permian granitic intrusions have been identified in the Chifeng area (Figure 2), namely, the Mingshan, Jianshanzi, Aohan Banner, Daluobogou, Xiaodonghuang, Beizifu, Shangchaoyanggou, Qixieyingzi, and Erdaogou plutons. Eight samples were collected from each of these plutons for geochronological analyses (Table 1) and twenty-four samples for geochemical analyses (Figure 2).

There are only two Early Permian granitoid intrusions in the study area, the Mingshan and Jianshanzi plutons. The Jianshanzi pluton, dominated by syenogranite, located at west of the Wutonghua Town of Chifeng City (Figure 2), intrudes into the Carboniferous Jiujuzi Formation, Permian Sanmianjing and Elitu Formations, and is covered by the volcanic rocks of the Baiyingaolao and Hannuoba Formations [22]. The Mingshan pluton, dominated by porphyritic biotite monzogranite, located at south of Laofu Town in Chifeng City (Figure 2), intrudes into the Late Devonian granite and is covered by the Cretaceous volcanic rocks [22].
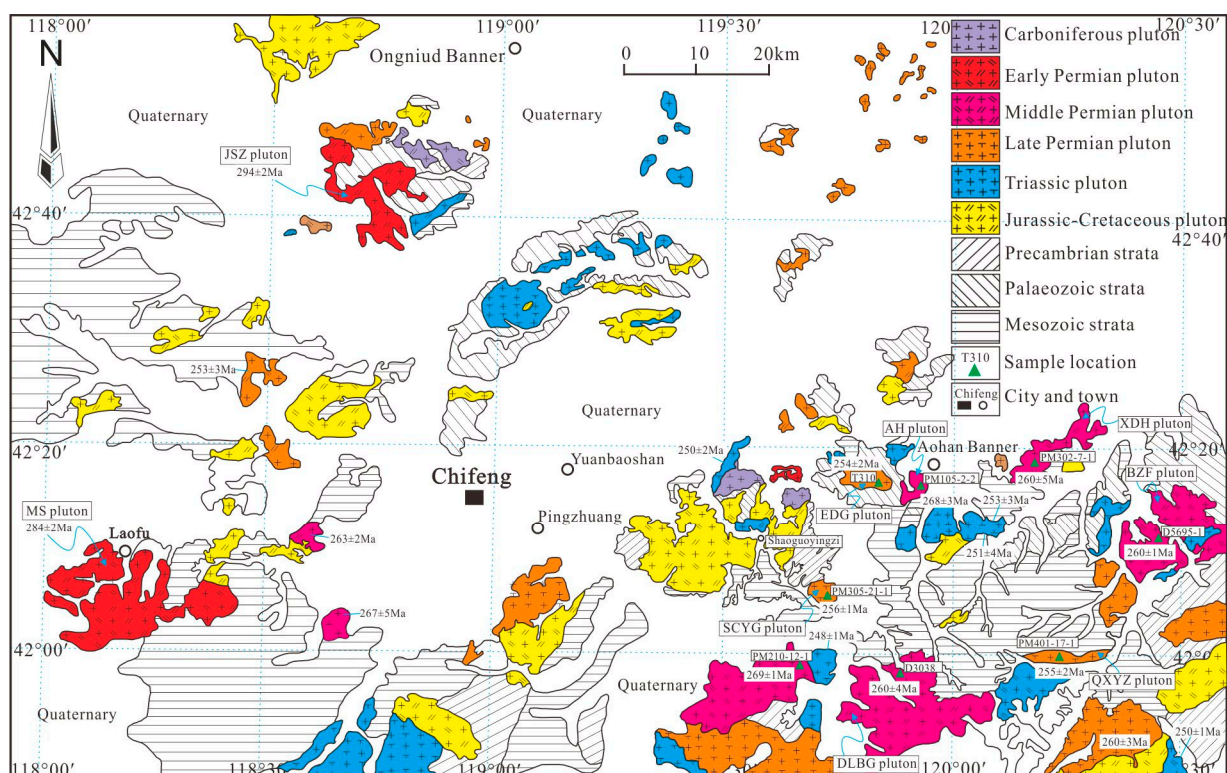
Figure 2. Simplified geological map of the study area in the north margin of the North China Craton showing sample locations, modified after [8]. AH–Aohan Banner, DLBG–Daluobogou, XDH–Xiaodonghuang, BZF–Beizifu, SCYG–Shangchaoyanggou, QXYZ–Qixieyingzi, EDG–Erdaogou.

Table 1. Location and lithology for the Permian granitic rocks of this study in the Chifeng area.

Sample No.	Name of Intrusion	Lithology	GPS Location	
PM210-12-1	Daluobogou pluton	monzogranite	119°41′28″	42°00′06″
PM105-2-2	Aohan Banner pluton	fine-grained biotite monzogranite	119°52′48″	42°17′58″
D3038	Daluobogou pluton	medium-grained monzogranite	119°51′53″	41°59′40″
PM302-7-1	Xiaodonghuang pluton	porphyry monzogranite	119°05′29″	42°19′21″
D5695	Beizifu pluton	medium-grained monzogranite	119°18′44″	42°07′51″
T310	Erdaogou pluton	medium-grained monzogranite	119°47′35″	42°18′50″
PM401-17-1	Qixieyingzi pluton	medium-grained syenogranite	119°08′56″	42°01′34″
PM305-21-1	Shangchaoyanggou pluton	monzogranite	119°42′24″	42°07′17″

The Aohan pluton, located west of Aohan Banner (Figure 2), is covered by the rhyolitic crystal tuff of the Upper Jurassic Manketouebo Formation and the andesitic tuff of the Lower Cretaceous Yixian Formation. This granitic pluton is dominated by monzogranites (samples PM105-2-1, PM105-2-2, PM105-2-3, PM105-2-4, PM105-2-4, and PM105-4-1) with a fine-grained granite texture and massive structure (Figure 3a). These samples are composed of potassium feldspar (34 wt%±), plagioclase (30 wt%±), quartz (30 wt%±), and biotite (5 wt%±), with accessory hematite, limonite, zircon, pyrite, and apatite (1 wt%±) (Figure 3b).

The Daluobogou pluton, located 80 km east of Chifeng City (Figure 2), is covered by the volcanic and sedimentary rocks of the Lower Cretaceous Yixian Formation. This pluton is dominated by monzogranites (samples PM210-12-1, D3038-1, D3038-2, D3038-3, D3047-1, D3048-1, and D3049-1) with fine-medium-grained texture and massive structure (Figure 3c,e). These samples consist of quartz (25 wt%±), plagioclase (28 wt%±), potassium feldspar (36 wt%±), and biotite (5 wt%±), with accessory limonite, zircon, and apatite (1 wt%±) (Figure 3d,f).
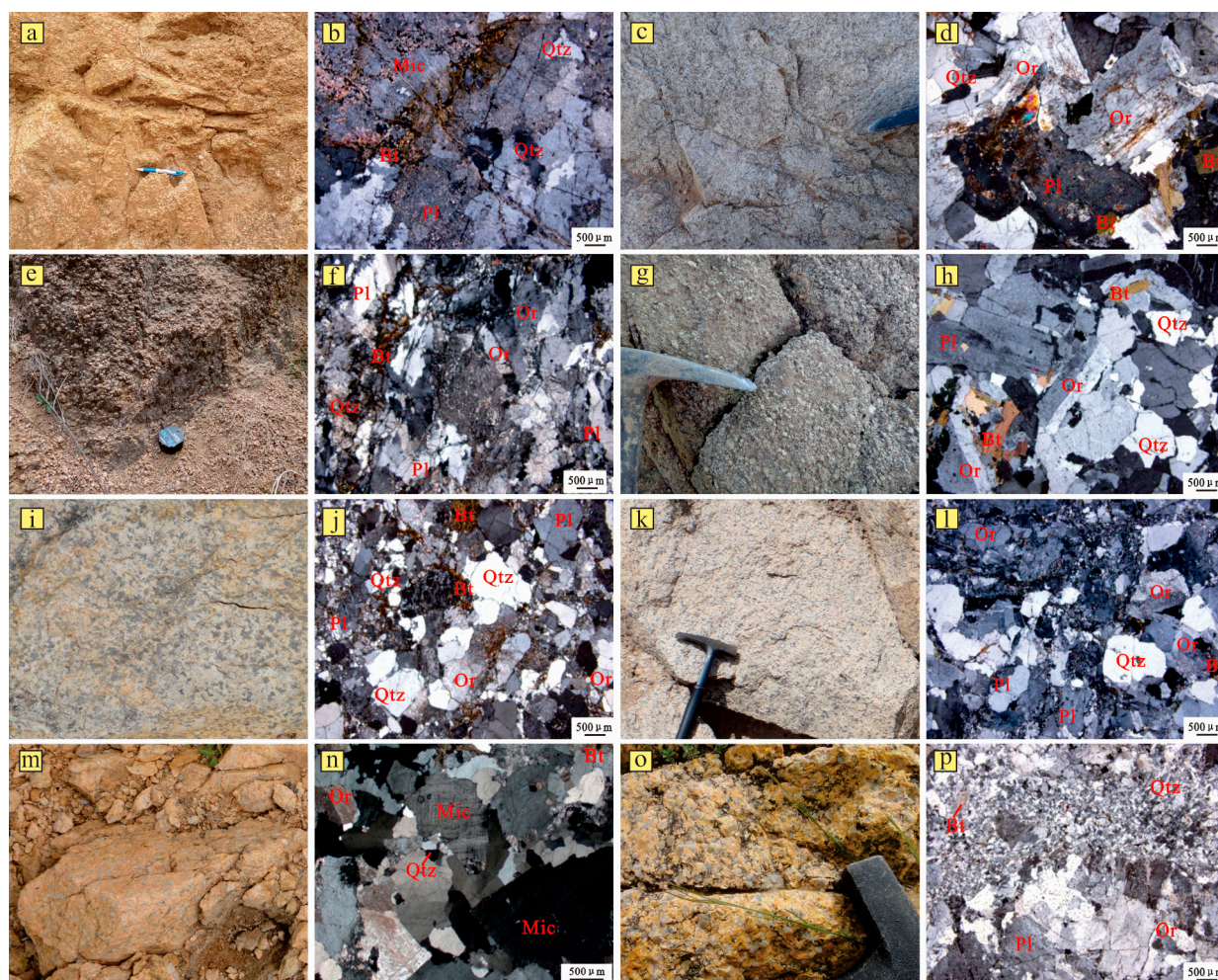
Figure 3. Outcrop pictures and microphotographs (cross-polarized light) of magmatic rocks from the Chifeng Area showing rock textures. (**a,b**) Aohan Banner pluton (fine-grained monzogranite); (**c,d**) Daluobogou pluton (fine-grained monzogranite); (**e,f**) Daluobogou pluton (medium-grained monzogranite) (**g,h**) Xiaodonghuang pluton (porphyritic biotite monzogranite); (**i,j**) Beizifu pluton (medium-grained monzogranite); (**k,l**) Shangchaoyanggou pluton(medium-grained monzogranite); (**m,n**) Qixieyingzi pluton (medium-grained syenogranite) and (**o,p**) Erdaogou pluton (medium-grained monzogranite); Qtz: quartz; Pl: plagioclase; Mic: microcline; Or: orthoclase; Bt: biotite.

The Xiaodonghuang pluton, located at Xiaodonghuang, Sijianfang, and Tengjiawopu in the northeast of Fengshou Town Aohan Banner (Figure 2), intrudes into the Upper Carboniferous Shizuizi Formation and is covered by the rhyolite and rhyolitic crystal tuff of the Upper Jurassic Manketouebo Formation. This pluton is dominated by biotite monzogranite (sample PM302-7-1) with porphyritic texture and massive structure (Figure 3g). The matrix is phanerocrystalline with medium-fine-grained granitic texture. These samples consist of quartz (25 wt%±), plagioclase (39wt%±), potassium feldspar (30 wt%±), and biotite (5 wt%±), with accessory zircon, magnetite, and titanite (1 wt%±) (Figure 3h).

The Bizifu pluton, located at Beizifu Town 30km east of the Aohan Banner (Figure 2), is intruded by the Mesozoic intrusions. This pluton is dominated by monzogranites (sample 5695-1) with massive structure and medium-fine-grained texture (Figure 3i). These samples consist of quartz (30 wt%±), plagioclase (32wt%±), potassium feldspar (34 wt%±), and biotite (3 wt%±), with accessory apatite, zircon, and titanite (1wt%±) (Figure 3j).

The Shangchaoyanggou pluton, located at Shangchaoyanggou, Yangjiaogou, and Weijiataizi in north of Jianping County (Figure 2), has fault contact with the Cretaceous Yixian Formation and the Sunjiawan Formation. This pluton is dominated by monzogranite

(sample PM305-21-1) with massive structure and fine-grained texture (Figure 3k). These samples consist of quartz (25 wt%±), plagioclase (25wt%±), potassium feldspar (44 wt%±), and biotite (5 wt%±), with accessory hematite, titanite, and zircon (1 wt%±) (Figure 3l). The minerals in this monzogranite showed a weak certain orientation in the northeast direction locally because of the influence of Nenjiang–Balihan Fault.

The Qixieyingzi pluton, located at Qixieyingzi, Jiangjiagou, and Guluyingzi in the southeast of Aohan Banner (Figure 2), is intruded by Cretaceous monzogranite and covered by volcanic rocks from the Lower Cretaceous Yixian Formation. This pluton is dominated by syenogranite (samples PM403-2-1, PM403-2-2, PM403-2-3, PM403-2-4, PM403-2-5, PM403-2-6) with massive structure and medium-grained texture (Figure 3m). These samples consist of potassium feldspar (55 wt%±), quartz (25 wt%±), plagioclase (15wt%±), and biotite (4wt%±), with accessory apatite, zircon, and titanite (1 wt%±) (Figure 3n).

The Erdaohou pluton, located at Erdaogou, Gaojiayaozi, and Sanlamayaozi 15km northwest of the Aohan Banner (Figure 2), intrudes into the Permian strata (i.e., the Sanmianjing, Elitu, and Yujiabeigou Formations) and is covered by rhyolite and andesite from the Lower Cretaceous Yixian Formation. This pluton is dominated by monzogranites (samples T310, PM103-2-1, PM103-2-3, PM103-4-2, PM103-6-1, PM103-6-2, PM103-6-4,) with massive structure and medium-grained texture (Figure 3o). These samples consist of potassium feldspar (36 wt%±), quartz (30 wt%±), plagioclase (30wt%±), and biotite (3 wt%±), with accessory zircon, magnetite, hematite, and limonite (1 wt%±) (Figure 3p).

3. Analytical Methods

3.1. Sample Preparation

After being collected from the field, samples for geochronological analyses were cleaned, crushed, and ground. Next, zircon crystals were separated from these samples by means of conventional heavy liquid and magnetic techniques, and the separates were hand-picked and purified under a binocular microscope at Langfang Yuneng Mineral Separation Co., Ltd. (Langfang, China). Next, the zircons were selected and embedded in epoxy resin and polished, then imaged through a scanning electron microscope via cathodoluminescence (CL) to reveal their internal structures. CL images of five samples (PM105-2-2, D3038, PM302-7-1, PM401-17-1, and T310) were obtained from the Zhongnan Mineral Supervision and Testing Center of the Ministry of Land and Resources, and the others (PM210-12-1, PM305-21-1 and D5659-1) from the electron microprobe Laboratory of the Institute of Geology and Geophysics, Chinese Academy of Sciences.

3.2. Zircon LA-ICP-MS U-Pb Isotope Dating

The U-Pb zircon ages for the Permian granites in the Chifeng area were obtained using an Agilent 7500a inductively coupled plasma–mass spectrometry (ICP-MS) instrument, equipped with a 193 nm ArF Excimer laser-ablation (LA) system. The spot size for the analyses was 36 μm, with an energy density of 8.5 J/cm^2 and repetition rate of 10 Hz. Helium was used as the carrier gas to transport the ablated material from the standard LA cells. Zircon 91500 (^{206}Pb/^{238}U age of 1062.4 ± 0.4 Ma (2σ) and ^{206}Pb/^{207}Pb age of 1065.4 ± 0.3 Ma (2σ)) was used as the external standard for age calibration, while standard silicate NIST 610 glass was used to calibrate content calculations [43]. Zircon standards TEMORA (^{206}Pb/^{238}U age of 416.78 ± 0.33 Ma (2σ), [44]) and QH (160 ± 1 Ma) were also used as secondary standards to monitor any deviation in age measurement. Isotopic ratios and element contents were calculated using Glitter software (version 4.0; Macquarie University, Sydney, Australia), and the age calculation and concordant plots were obtained using Isoplot (v. 3.0) [45]. Common Pb was corrected using the method described by Andersen (2002) [46]. The analytical data are presented on U-Pb concordia diagrams with 1σ errors, and the mean ages are weighted means at the 95% confidence level [47]. Analyses of five samples (PM105-2-2, D3038, PM302-7-1, PM401-17-1, and T310) were conducted at the Zhongnan Mineral Supervision and Testing Center of the Ministry of

Land and Resources, and the others (PM210-12-1, PM305-21-1, and D5659-1) at the Geologic Laboratory Center, China University of Geosciences (Beijing, China). The analytical results are listed in Table S1.

3.3. Major- and Trace-Element Analyses

Next, major-, trace- and rare-earth-element (REE) analyses for 24 samples were conducted at the Northeast China Supervision and Inspection Center of Mineral Resources, Ministry of Land and Resources (Shenyang, China). After petrographic examination and removal of altered rock surfaces, the samples were crushed and ground to 74 μm in an agate mill. Then, whole-rock major-element contents were determined using X-ray fluorescence spectrometry (XRF), yielding analytical precisions exceeding 2%. The trace-element and REE contents were determined using ICP-MS and yielded analytical precisions exceeding 5% for elements with contents of >10 ppm, exceeding 8% for elements with contents of <10 ppm, and 10% for the transition metals. The results are listed in Table S2.

4. Analytical Results

4.1. Zircon U-Pb Ages

4.1.1. Early-Middle Permian

Sample PM210-12-1 is a monzogranite with fine-grained texture collected from the Daluobogou pluton in the Machang area. Zircons within this sample are generally colorless, transparent, and mostly subhedral to euhedral columnar in shape. They have length-to-width ratios of 3:2 to 4:1. In the cathodoluminescence (CL) images (Figure 4), most grains display fine-scale oscillatory growth zoning and clear internal structure. The zoning, combined with Th/U ratios of 0.42–1.57 (Table S1), indicates a magmatic origin [48,49]. A total of 24 isotopic analyses were conducted on 24 zircons grains from this sample. Most of the analyses are concordant and define a weighted mean $^{206}Pb/^{238}U$ age of 269 ± 1 Ma (MSDW = 0.90) (Figure 5a), which is interpreted as the crystallization age of the monzogranite.
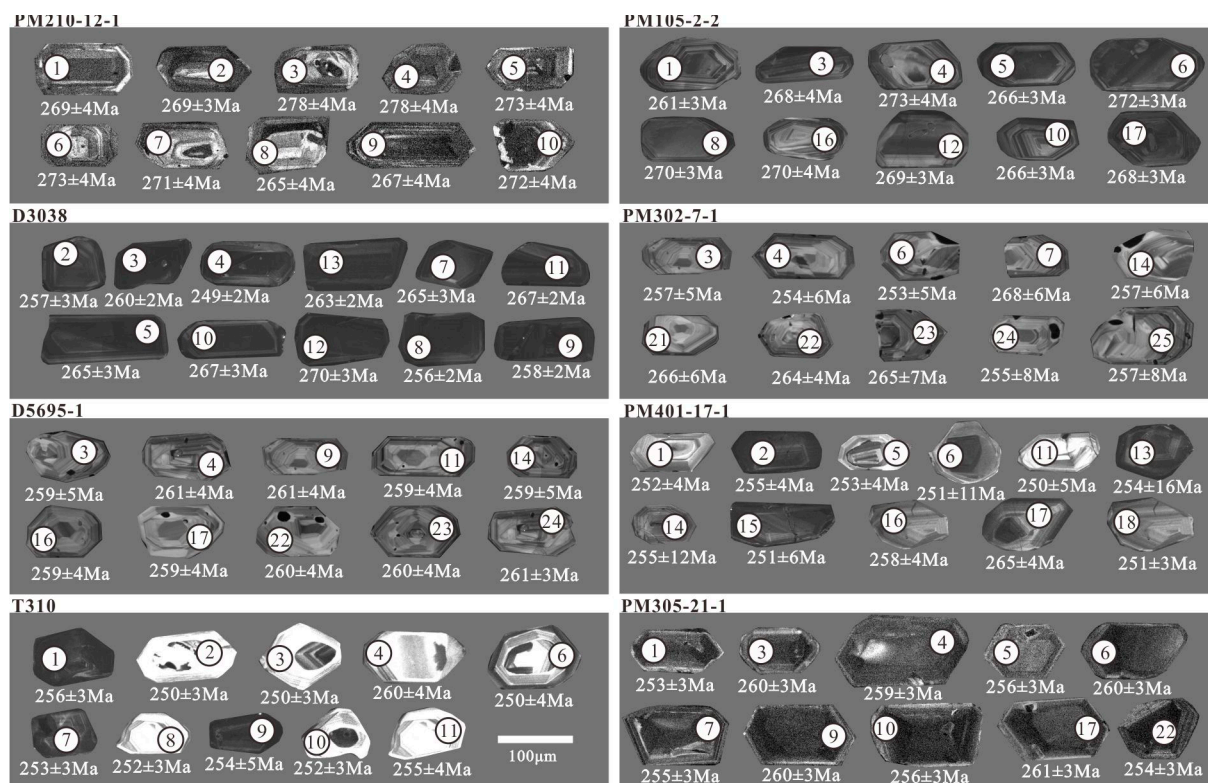

Figure 4. Cathodoluminescence (CL) images of selected zircon grains from the Permian granites in this study.
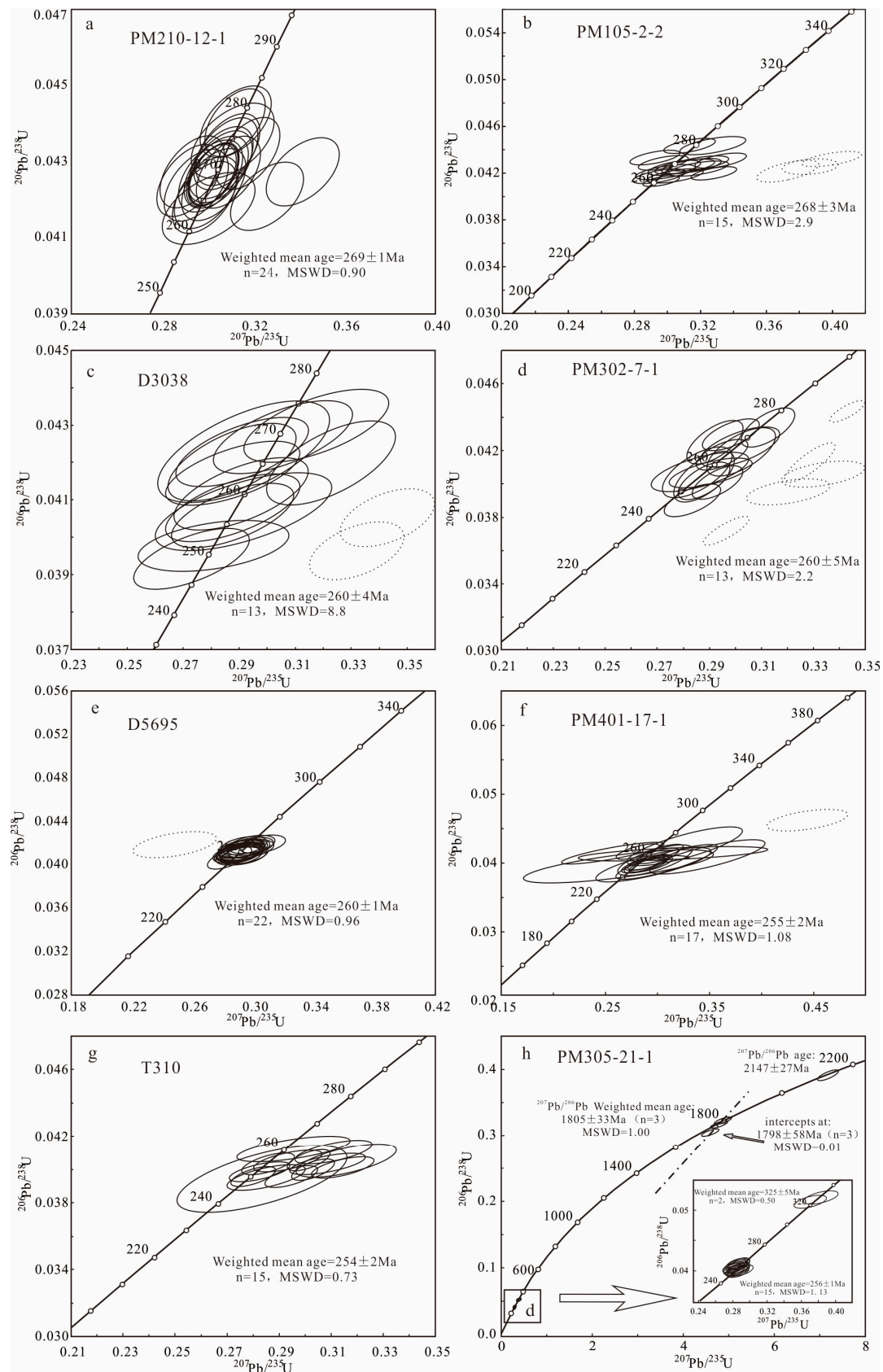
Figure 5. Zircon $^{207}Pb/^{235}U$-$^{206}Pb/^{238}U$ concordia diagrams of the Permian granites samples from this study. The dashed ellipse represents the discordant age. (**a**): PM210-12-1; (**b**): PM105-2-2); (**c**): D3038; (**d**): PM302-7-1; (**e**): D5695; (**f**): PM401-17-1; (**g**): T310; (**h**): PM305-21-1.

Sample PM105-2-2, a fine-grained biotite monzogranite, was collected from the Aohan pluton. Zircons from this sample are translucent and euhedral to subhedral or form short prisms to long columns in shape. They have length-to-width rations ranging from 2:1 to 3:1. CL imaging reveals that most zircons are bright with fine-scale oscillatory growth zoning (Figure 4), indicating a magmatic origin [48,49]. A total of 18 analyses were made on 18 zircons, which were shown to have high Th/U ratios (0.43–0.88) (Table S1). Three analysis points were not considered in the concordia diagram due to the low confidence (less than 90%) (Figure 5b). The remaining 15 analysis points were plotted on or near the concordia line. The concordant zircon data give a weighted mean $^{206}Pb/^{238}U$ age of 268 ± 3 Ma (MSDW = 2.90), interpreted as the crystallization age of the sample.

4.1.2. Late-Middle Permian

Sample D3038 is a medium-grained monzogranite from the Daluobogou pluton near the Luofugou area. The zircon grains from the sample are mostly euhedral elongate prisms with oscillatory zoning. They have length-to-width ratios of 2:1 to 4:1, and Th/U ratios of 0.52 to 1.31 (Figure 4), indicating magmatic origin [48,49]. A total of 15 analyses on 15 zircon grains were conducted. All but two of the analyses were concordant and yield a weighted mean $^{206}Pb/^{238}U$ age of 260 ± 4 Ma (MSDW = 8.8) (Figure 5c), which is regarded as the monzogranite's emplacement age.

Sample PM302-7-1, a porphyry monzogranite, was collected from the Xiaodonghuang pluton of Fengshou Village, Aohan Banner. Zircon grains from this sample are prismatic and stubby in shape, and the Th/U ratios mostly cluster around 0.43–1.38 (Table S1). A total of 23 analyses were conducted on 23 zircons; 10 analyses were excluded because of high discordancy, and the remaining 13 analysis spots yielded a weighted mean $^{206}Pb/^{238}U$ age of 260 ± 1 Ma (MSDW = 0.96) (Figure 5d), which is considered as representing the crystallization age of porphyritic monzogranite.

Sample D5695, a medium-grained monzogranite, was collected from the Beizifu pluton. Zircons from this sample are generally colorless, transparent, and euhedral in shape. In the CL images, most of them display fine-scale oscillatory zoning, with high Th/U ratios of 0.29–1.35, indicating magmatic origin [48,49]. A total of 25 spots were analyzed on 25 zircons from this sample; 3 analyses were excluded due to high discordancy, and the remaining 22 spots were concordant. The concordant zircon data give a weighted mean of $^{206}Pb/^{238}U$ age of 260 ± 1 Ma (MSDW = 0.96) (Figure 5e), interpreted as the sample's emplacement age.

4.1.3. Late Permian

Sample PM401-17-1, a medium-grained syenogranite, was collected from the Qixiey-ingzi pluton. Zircons within sample PM401-17-1 are generally euhedral and prismatic with length-to-width ratios of 2:1–4:1. They show variable degrees of oscillatory zoning visible during CL imaging (Figure 4) and have Th/U ratios of 0.43–2.83 (Table S1), characteristic of magmatic zircons of acid rocks [48,49]. Excluding three discordant data points likely caused by lead loss, the remaining 17 analysis spots yielded a weighted mean $^{206}Pb/^{238}U$ age of 255 ± 2 Ma (MSDW = 1.08) (Figure 5f), which is interpreted to be the crystallization age of the syenogranite.

Sample T310, a medium-grained monzogranite, was collected from the Erdaogou pluton. Zircon grains within this sample are generally colorless, transparent, and short columnar in shape, with a maximum length-to-width ratio of 2:1. The CL imaging reveals that most grains have fine oscillatory zones (Figure 4). These properties, together with their relatively high Th/U ratios (0.43–2.97) (Table S1), suggest the zircons are of magmatic origin [48,49]. The results of all 15 analyses are consistent and define a weighted mean $^{206}Pb/^{238}U$ age of 254 ± 2 Ma (MSDW = 0.73) (Figure 5g), which is interpreted as the time of crystallization of the monzogranite.

Sample PM305-21-1 is a monzogranite collected from the Shangchaoyanggou pluton. Zircons from this sample are generally euhedral and prismatic with length-to-width ratios

of 2:1 to 3:1. In the CL images, most grains display fine-scale oscillatory growth zoning (Figure 4), with high Th/U values of (0.28–1.92) (Table S1). A total of 23 spots were analyzed on 23 zircons from this sample; 2 analyses were excluded due to high discordancy, and the remaining 21 analysis points were plotted on or near the concordant line, and gave four groups of ages (Figure 5h). The first group comprises one analysis (No. 16) with a $^{207}Pb/^{206}Pb$ age of 2147 ± 27 Ma, representing a middle Paleoproterozoic magmatic event. The second group consists of three analyses (Nos. 11, 18, 20), yielding a weighted mean $^{207}Pb/^{206}Pb$ age of 1,805 ± 33 Ma, which is consistent with their upper intercept age of 1798 ± 58 Ma, representing late Paleoproterozoic magmatic activity. The third group comprises two analyses (Nos. 14 and 15), yielding a weighted mean $^{206}Pb/^{238}U$ age of 352 ± 5 Ma (MSDW = 0.50) (Figure 5h). The fourth group comprises 15 analyses, yielding a weighted mean $^{206}Pb/^{238}U$ age of 256 ± 1 Ma (MSDW = 1.13). The youngest age of 256 ± 1 Ma is interpreted to be the emplacement age of the monzogranite, whereas the other three ages (ca. 2147, 1805, and 352 Ma) are interpreted to represent the crystallization ages of captured zircon entrained by the granitic magma.

4.2. Major and Trace Element Geochemistry

4.2.1. Early-Middle Permian Monzogranite

The monzogranites are high in SiO_2 (72.00–73.37 wt%), K_2O (4.32–4.70 wt%), and ($Na_2O + K_2O$) (14.17–14.62 wt%), with Na_2O/K_2O ratios of 0.88–1.01, yet low in TiO_2 (0.12–0.20 wt%), MnO (0.02–0.03 wt%), MgO (0.04–0.15 wt%), and P_2O_5 (0.04–0.07 wt%) (Table S2). They are classified in the alkalic series, and assigned to the high-K calc-alkaline igneous rocks (Figure 6a). Their A/CNK (molar $Al_2O_3/(CaO + Na_2O + K_2O)$) values range from 1.08 to 1.23, indicative of weakly peraluminous granites (Figure 6b). The total rare earth elements (REEs) range from 143.96 to 156.29 µg/g (with the exception of one datum lower than 66.45 µg/g). In the chondrite-normalized REE diagram (Figure 7a), the monzogranite samples have a pattern of slightly enriched LREEs but flat HREEs, with $(La/Yb)_N$ and ΣLREE/ΣHREE (total light rare-earth elements versus total heavy rare-earth elements) ratios of 3.54–19.62 and 5.29–10.06 and moderately negative Eu anomalies (Eu/Eu* = 0.42–0.57). In the primitive-mantle (PM) normalized trace element diagram (Figure 7b), all samples show negative Ba, Nb, Sr, P, and Ti anomalies and are all enriched in Rb, Th, K, La, Zr, and Hf.
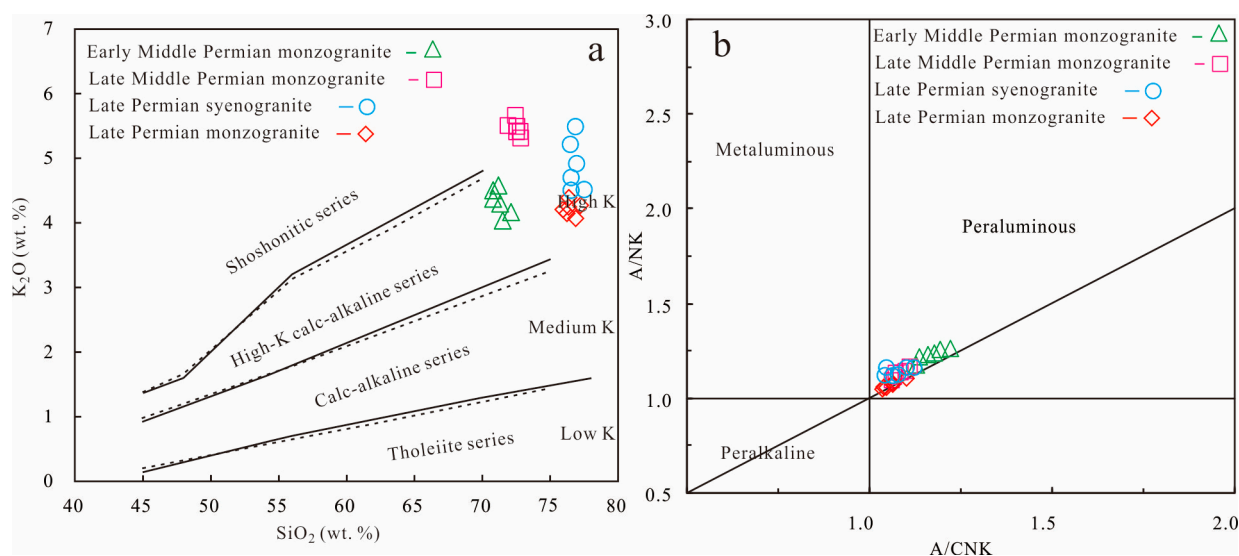

Figure 6. K_2O versus SiO_2 (**a**) and A/NK (molar/molar) versus A/CNK (molar/molar) (**b**) diagrams for Permian granitic rocks. Normalization values are from [50] and [51], respectively.
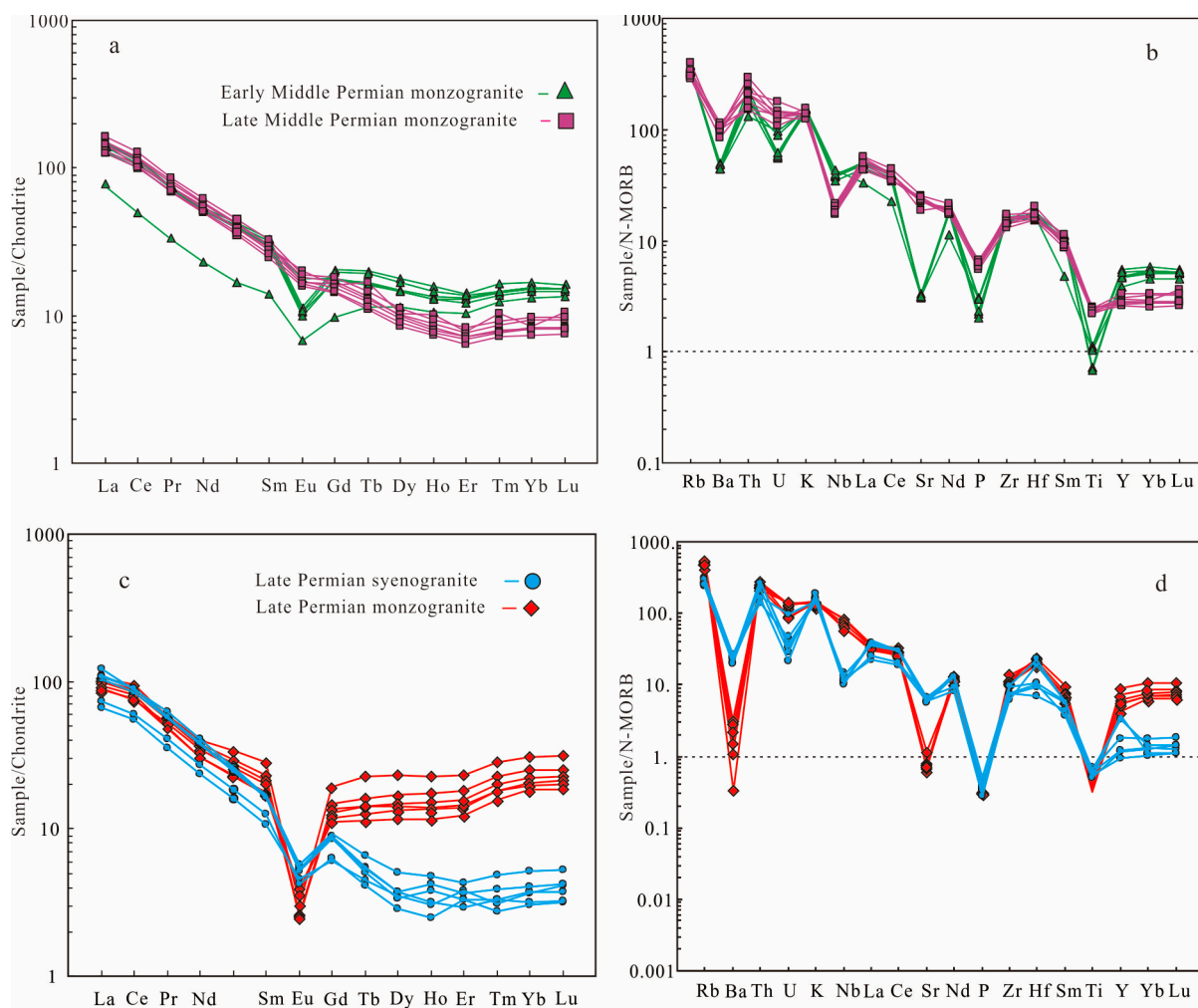
Figure 7. Chondrite-normalized REE patterns (**a**,**c**) and primitive mantle-normalized trace element spider diagrams (**b**,**d**) for these Permian granitic rocks in the Chifeng area. The values of chondrite and primitive mantle are from [52].

4.2.2. Late-Middle Permian Monzogranite

All of the monzogranite samples are alkalic- and silica-rich high-K calc-alkaline igneous rocks (Figure 6a). The whole-rock analysis results yield SiO_2 = 73.40–74.11 wt%, Na_2O/K_2O ratios = 0.65–070, and total $Na_2O + K_2O$ = 9.30–9.76. The samples are low in TiO_2 = 0.16–0.18 wt%, MnO = 0.03–0.04 wt%, MgO = 0.20 wt%, and P_2O_5 = 0.03 wt% (Table S2). They are classified as potassium basalt series and weakly peraluminous granites, due to their respective A/CNK, K_2O, and Al_2O_3 values of 1.07–1.11, 5.47–5.80 wt%, and 13.93–14.21 wt% (Figure 6b). The total REEs range from 272.5 to 340.64 μg/g. The chondrite-normalized REE diagrams invariably show a relative enrichment in LREEs, with $(La/Yb)_N$ and ΣLREE/ΣHREE ratios of 19.58–26.88 and 18.36–20.38, and moderate to significant negative Eu anomalies with Eu/Eu* ratios of 0.31–0.41 (Figure 7a). Furthermore, in the PM-normalized trace element diagram (Figure 7b), the rocks are enriched in large ion lithophile elements (LILEs; e.g., Rb, Th, K, La, and Ce) and depleted in high field-strength elements (HFSEs; e.g., Nb, P, and Ti). Finally, all samples show negative Ba anomalies.

4.2.3. Late Permian Monzogranite and Syenogranite

The Late Permian monzogranites have SiO_2 = 76.29–77.30 wt% and contain Al_2O_3 of 12.75–12.93 wt%, TiO_2 of 0.06–0.07 wt%, MnO of 0.01–0.08 wt%, MgO of 0.11 wt%, P_2O_5 of 0.01 wt%, and total $Na_2O + K_2O$ of 8.40–8.79 wt%, with Na_2O/K_2O ratios of 0.95–1.09 (Table S2). They are classified as the weakly peraluminous high-K calc-alkaline

series on a plot of K_2O against SiO_2 (Figure 6a), and plot in the peraluminous field in the A/CNK vs. A/NK diagram (Figure 6b). The total REEs range from 101.75 to 128.91 μg/g. In the chondrite-normalized REE diagram, they are weakly fractionated, with $(La/Yb)_N$ and ΣLREE/ΣHREE ratios of 3.28–5.06 and 4.73–7.25 and strong negative Eu anomalies (Eu/Eu* = 0.13–0.28) (Figure 7c). In the PM-normalized trace-element diagram (Figure 7d), they show similar patterns, albeit with notable differences in the absolute element concentrations. All samples are enriched in Rb, Th, U, K, Nd, Zr, and Hf, but depleted in Ba, Sr, P, and Ti.

The Late Permian syenogranites are high in SiO_2 (76.22–77.58 wt%) and K_2O (4.35–5.62 wt%), but low in Al_2O_3 (12.05–12.63 wt%), TiO_2 (0.09–0.16 wt%), MnO (0.01–0.05 wt%), MgO (0.20–0.56 wt%), and P_2O_5 (0.01–0.02 wt%). They are high-K calc-alkaline, and weak peraluminous igneous rocks (Figure 6a), with total $Na_2O + K_2O$ of 0.49–0.86, and A/CNK ratios ranging from 1.05 to 1.16 (Figure 6b). All but two have high total REEs, with the total REE values ranging from 107.94 to 215.80 μg/g. The chondrite-normalized REE diagram shows that they are enriched in LREEs, with $(La/Yb)_N$ and ΣLREE/ΣHREE ratios of 18.05–32.16 and 16.77–25.86, respectively (Figure 7c). The granites also have moderately negative Eu anomalies (Eu/Eu* = 0.39–0.54). Finally, the PM-normalized trace-element diagram shows that they are enriched in LILEs (e.g., Rb, Th, K, La, and Ce) and LREEs (e.g., Nd, Zr, and Hf), and depleted in HFSEs (e.g., Ba, Nb, P, Ti, and Sr) (Figure 7d).

5. Discussion

5.1. Permian Magmatism in the Chifeng Area

Previous research on the Permian magmatism in the Chifeng area has been quite scarce, only covering the granodiorite located in the Late Permian in Mengguyingzi [15], diorite (256 ± 6 Ma) in Chaihuyingzi [53], gneissic monzogranite in the Liangjin mining area of Jinchanggou (249 ± 1 Ma) [40], Early Permian monzogranite in the Mingshan pluton, and syenite in the Jianshanzi pluton (284.4 ± 7.9 Ma, 294.7 ± 8.5 Ma) [22]. The coeval volcanic rocks include the andesite of the Permian Elitu Formation exposed in the Mingshan uplift belt in the west of Chifeng (273 Ma). Based on the available data, combined with those of this study, the Permian granitic chronology framework was established in the Chifeng area (Table 2).

Table 2. Geochronological data for the Permian granitic rocks in the Chifeng area.

Order	Sample	Pluton	Lithology	Age (Ma)	Method	References
1	14CH10	Jianshanzi	Monzogranite	294 ± 2	LA-ICPMS	[22]
2	14CH24	Mingshan	Granodiorite	284 ± 2	LA-ICPMS	[22]
3	PM210-12-1	Daluobogou	Monzogranite	269 ± 1	LA-ICPMS	This study
4	PM105-2-2	Aohan Banner	Monzogranite	268 ± 3	LA-ICPMS	This study
5	D3038	Daluobogou	Monzogranite	260 ± 4	LA-ICPMS	This study
6	PM302-7-1	Xiaodonghuang	Monzogranite	260 ± 5	LA-ICPMS	This study
7	D5695-1	Beizifu	Monzogranite	260 ± 1	LA-ICPMS	This study
8		Sidaogou	Syenogranite	267 ± 5	LA-ICPMS	
9		Jianshanzi	Monzogranite	263 ± 2	LA-ICPMS	Inner Mongolia 1:250,000 Chifeng
10		Majiadi	Granite	274 ± 4	LA-ICPMS	regional geological survey
11		Zhaojiawopu	Diorite	253 ± 3	LA-ICPMS	
12	PM305-21-1	Shangchaoyanggou	Granodiorite	256 ± 1	LA-ICPMS	This study
13	PM401-17-1	Qixieyingzi	Syenogranite	255 ± 2	LA-ICPMS	This study
14	T310	Erdaohou	Monzogranite	254 ± 2	LA-ICPMS	This study
15	T101	Mengguyingzi	Granodiorite	251 ± 4	LA-ICPMS	[8]
16	D2711-1	Xiaxinjing	Monzogranite	250 ± 2	LA-ICPMS	[8]
17	PM210-6-1	Daluobogou	Monzogranite	248 ± 1	LA-ICPMS	[8]
18	CH2	Chaihulanzi	Diorite	257 ± 6	SHRIMP	[53]
19	DJ10-18	Shuangjingzi	Granite	278 ± 1	LA-ICPMS	[54]
20	PM003-1	Mengguyingzi	Granodiorite	253 ± 3	LA-ICPMS	[15]
21		Dayingzi	Syenogranite	268 ± 3	LA-ICPMS	[55]
22	XG01	Jinchanggouliang	Monzogranite	250 ± 1	LA-ICPMS	[40]

5.1.1. Early Permian (294–284 Ma)

The magmatic activities are intense in the Permian in the northern margin of the NCC. However, these magmatic activities are mainly concentrated in the central region of Inner Mongolia and are rare in the Chifeng area. The Early Permian granite studied in this paper includes the syenite in the Jianshanzi pluton (294 Ma) and the monzogranite in the Mingshan pluton (284 Ma), indicating that the Early Permian granite of the Chifeng area formed during 294–284 Ma [22].

5.1.2. Middle Permian (269–260 Ma)

Late Paleozoic magmatic rocks are linearly distributed in the study area and its adjacent area, among which the Middle Permian magmatic rocks are the most widely distributed. They are exposed on the northern margin of the NCC and XMOB. In the Chifeng area, rocks that have been identified include syenogranite (269 ± 1 Ma) and monzogranite (260 ± 4 Ma) in the Daluobogou pluton, fine-grained monzogranite in Aohan Banner (268 ± 3 Ma), porphyritic medium-coarse monzogranite in Xiaodonghuang (260 ± 5 Ma), and medium-grained monzogranite in Beizifu (260 ± 1 Ma). The syenogranite at the margin of the Dayingzi pluton in the northwestern Chifeng has an age of 268 ± 3 Ma [55]. The geochronological results show that the Middle Permian intrusive rocks formed between 269 and 260 Ma, indicating that magmatism occurred in the Chifeng area in this period.

5.1.3. Late Permian-Early Triassic (256–248 Ma)

The Late Permian-Early Triassic granitic magmatism in the study area occurred frequently in the same tectonic background, and the volcanic activity in the Early Triassic was a continuation of that in the Late Permian [13,37]. The Late Permian granitic rocks identified in the research area include the weak gneissic monzogranite of the Shangchaoyanggou pluton (256 ± 1 Ma), the medium-grained syenogranite of the Qixieyingzi pluton (255 ± 2 Ma), and medium-grained monzogranite of the Erdaogou pluton (253 ± 2 Ma). There are also many other magmatic activities, such as the diorite hosting the granulite in Chaihuyingzi (257 ± 6 Ma) [53], fine-grained granodiorite in Mengguyingzi (252 ± 2 Ma) [15], gneissic monzonite in the Liangjin mining area of Jinchanggou (249 ± 1 Ma) [40], fine-grained granodiorite in the Mengguyingzi pluton (251 ± 2 Ma), medium-grained monzogranite in the Xiaxinjing pluton (250 ± 2 Ma), and medium-grained syenogranite in the Daluobogou pluton (247 ± 1 Ma) [8]. The zircon U-Pb ages of these granitic intrusions range from 256 to 247 Ma, indicating that the most intense magmatism occurred in the Late Permian-Early Triassic.

5.2. Genetic Types of the Middle-Late Permian Granitic Rocks in the Chifeng Area

5.2.1. Middle Permian Monzogranite

The early Middle Permian monzogranite (269 ± 1 Ma) is alkali-rich and high-potassium, calc-alkaline rock, and is rich in Si and Al. The A/CNK is between 1.08 and 1.23, indicating that it is peraluminous. The fine-grained monzogranite is aluminum-saturated, high-potassium, calc-alkaline rock. ΣREE is low, and close to the average level of the continental crust. Europium is moderately depleted. All of these granites fall in the range of classic island arc rocks in the $(La/Yb)_N$–Yb_N diagram and Y–Sr/Y diagram (Figure 8). By comparing the trace element ratio of fine-grained monzogranite to that of the continental crust average value and differentiated granite, it is concluded that the monzogranite of this phase is I-type granite.

The late Middle Permian monzogranite is alkali-rich, high-potassium, calcium-alkaline rock, rich in Si, with medium Al. The A/CNK value is between 1.07 and 1.11, indicating that it is slightly peraluminous. The medium-grained monzogranite is slightly aluminum-saturated, alkali-rich, high-potassium, calc-alkaline rock. The ΣREE content is much higher than the average level of the continental crust. Europium is moderately depleted, and these samples fall in the range of classic island arc rocks in the $(La/Yb)_N$–Yb_N and Y–Sr/Y diagrams (Figure 8). By comparing the trace-element ratio of medium-grained

monzogranite to that of the continental crust average value and differentiated granite, it is concluded that this monzogranite in the Daluobogou pluton is I-type granite.
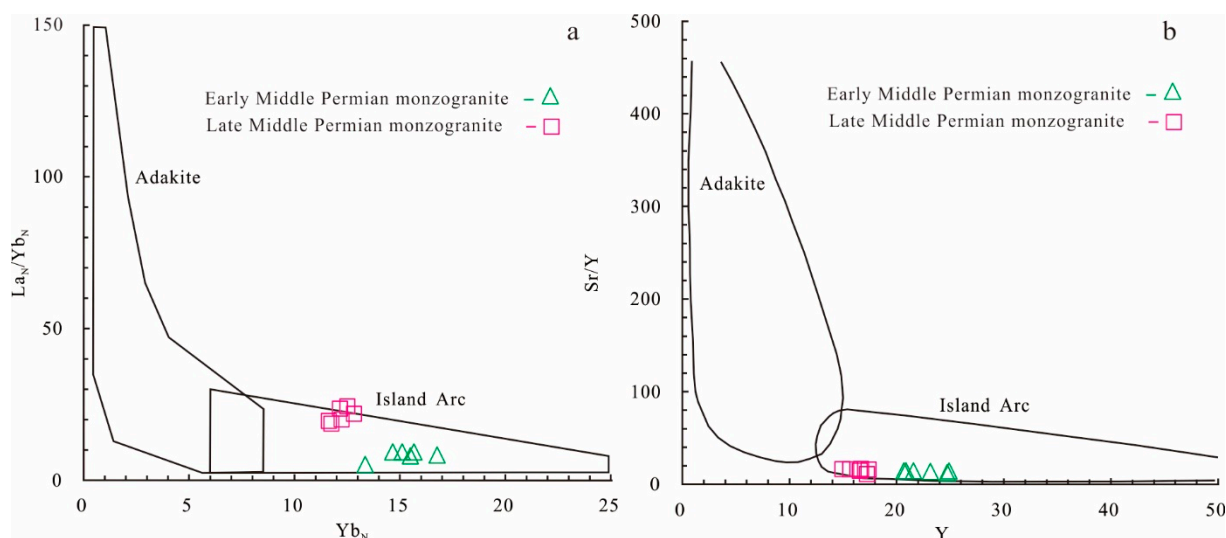

Figure 8. (a) La_N/Yb_N versus Yb_N; (b) Sr/Y versus Y diagram of the Middle Permian granites in Aohan area, modified after [56].

5.2.2. Genesis of the Late Permian Granite

The geochemistry characteristics show that the Late Permian monzogranite is alkali-rich, high-potassium, calc-alkaline rock, rich in Si and poor in Al. The A/CNK value is in the range of 0.95–1.05, indicating moderately peraluminous rock. The monzogranite belongs to alkali-rich, medium-Al, high-potassium, calc-alkaline rock. ΣREE is close to the average level of the continental crust. The trace elements have similar characteristics to those of A-type granite [57]. The light and heavy rare-earth elements are obviously fractionated, with strongly negative Eu anomalies. The rare-earth element distribution pattern forms a "V" shape. A-type granite has high heavy rare-earth elements and Zr, Nb, Ce, and Y content levels due to their rich alkalinity [57]. The observed enrichment of heavy rare-earth elements show high contents of high field-strength elements such as Nb, Zr, and Hf, yet low Sr and Ba contents (Figure 7), showing the characteristics of A-type granite. In the 10,000 Ga/Al-Zr, 10,000 Ga/Al-Nb, and 10,000 Ga/Al-Na_2O + K_2O diagrams (Figure 9a, Figure 9b, and Figure 9c, respectively) of the Late Permian intrusive rocks, the monzogranite falls in the range of A-type granite. The (Zr + Nb + Ce + Y) content of the monzogranite is low (288.49–354.33 µg/g, less than 350 µg/g [57]), being slightly lower than the (Zr + Nb + Ce + Y) value of A-type granite (usually greater than 350 µg/g); however, there were some exceptions [58]. This puts the rock in the range of A-type granite in the (Zr + Nb + Ce + Y)–(K_2O + Na_2O)/CaO diagram (Figure 9d). Zhang et al. (2012) suggested that A-type granite should be distinguished based on the comprehensive analyses of the (Zr + Nb + Ce + Y), rare-earth-element and trace-element diagrams rather than the (Zr + Nb + Ce + Y) diagram alone [57]. The most important geochemical characteristics of A-type granite are rich in SiO_2 (usually >70%, mostly >75%); rich in K_2O (4–6% or higher); depleted in Al_2O_3 (content of 12–13%), Sr, Ba, Eu, Ti, and P; and a "V"-shaped REE pattern with an obviously negative Eu anomaly [57]. The monzogranite has a SiO_2 content of 76.32–77.20%, a K_2O content of 4.15–4.47%, and an Al_2O_3 content of 12.77–12.93%, showing negative anomalies of Sr, Ba, Ti, and P. The monzogranite has a rare-earth element distribution pattern of a "V" shape with an obviously negative Eu anomaly, which is the same as the A-type granite distributed in northeastern China [6]. A-type granite is generally formed in high-temperature environments [57]. With the Zr saturation temperature of 807–828 °C, the monzogranite in the EDG pluton is not high-temperature granite. However, experimental petrology shows that when the pressure is less than 0.5 GPa and the water

content is 1–6%, then the partial melting temperature of A-type granite can be reduced to 800–830 °C [59], or even lower [60–62]. In summary, it is concluded that the Late Permian monzonitic granite can be classified as A-type granite.
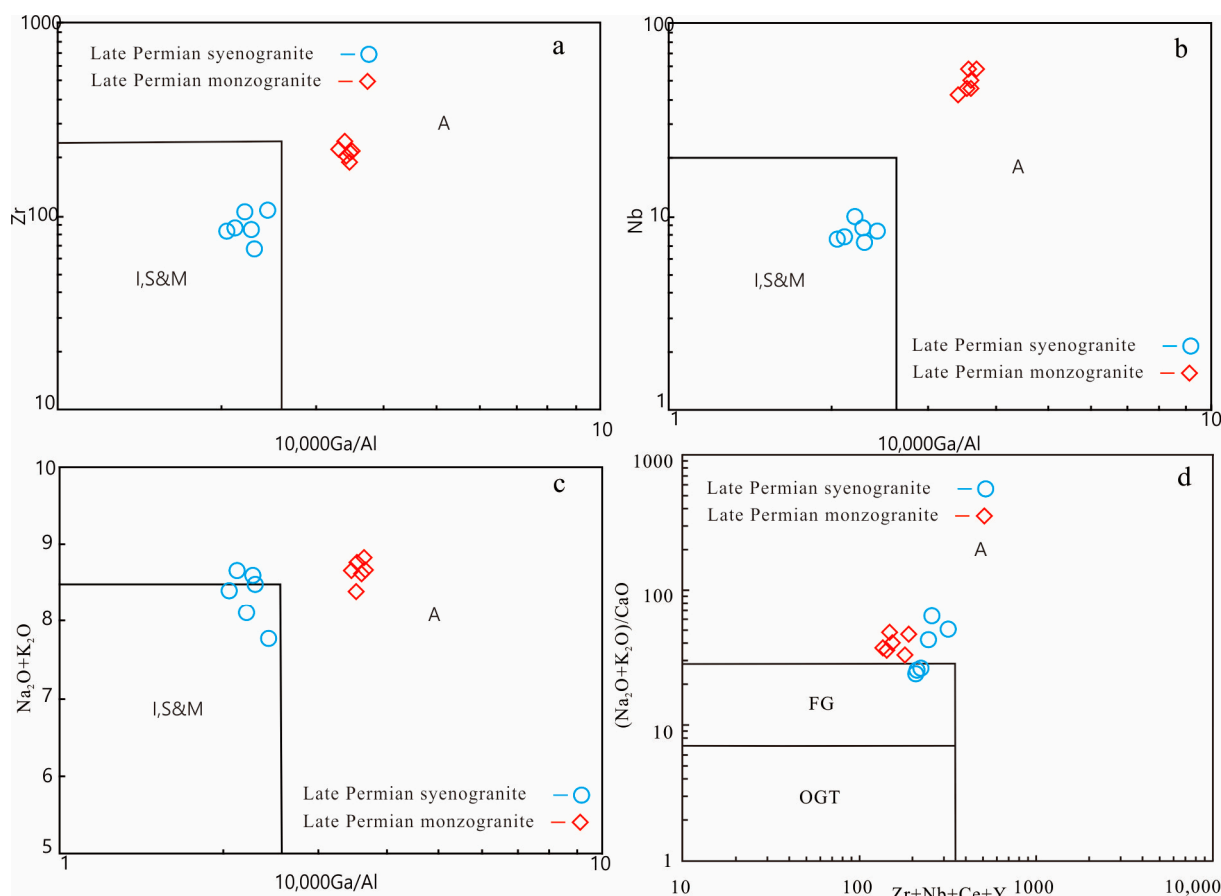

Figure 9. Diagram of 10,000 Ga/Al vs. Zr, Nb, Na$_2$O + K$_2$O (**a**–**c**), and (Zr + Nb + Ce + Y) vs. (Na$_2$O + K$_2$O/CaO) (**d**) for the Late Permian granitic intrusions [56]. A, A-type granite; FG, highly fractionated I-type granite; I, S&M, OGT, unfractionated I, S, and M-type granite.

The syenogranite is high-potassium, calc-alkaline rock, rich in Si, and depleted in Al. The A/CNK value is in the range of 1.05–1.16, indicating slight peraluminum. The content of the ΣREE is close to the crust average level and the existing Eu moderately negative anomaly. The syenogranite does not fall in the range of A-type granite in the 10,000 Ga/Al–Zr and 10,000 Ga/Al–Nb diagrams (Figure 9). The syenogranite presented here shows the characteristics of A-type granite, with SiO$_2$ content of 76.22–77.58%, K$_2$O content of 4.35–4.87%, Al$_2$O$_3$ content of 12.05–12.56%, and negative anomalies of Sr, Ba, Eu, Ti, and P [57]. The samples fall in the transitional range of I-, S-, and A-type granite in the 10,000 Ga/Al–Na$_2$O + K$_2$O diagram (Figure 9a–c), but in the range of A-type granite in the (Zr + Nb + Ce + Y)–(K$_2$O + Na$_2$O)/CaO diagram (Figure 9d). In the standardized diagram of chondrite-normalized REE patterns (Figure 7c), the syenogranite does not show the "V"-shaped pattern or obviously negative Eu anomaly, which is inconsistent with the characteristics of A-type granite [6]. Combined with its relatively low content of (Zr + Nb + Ce + Y) (132.44–185.68 μg/g), it is considered that the syenogranite belongs to I-type rather than A-type granite.

5.2.3. Petrogenesis of High-K, I-Type Granitic Rocks of the Permian

As discussed above, both the Middle Permian monzogranite and Late Permian syenogranite in the Chifeng area are high-K calc-alkaline I-type granite, and the origins of such granite are still under debate [63,64]. Some geologists uphold the model of fractional

crystallization and crustal assimilation of mantle-derived basaltic magma [65,66], while some insist on the model of mixing of crust-derived and mantle-derived magmas [67–70], and still others attribute the model of partial melting of hydrous medium- to high-K andesitic to basaltic meta-igneous rocks under crustal conditions [63,71,72].

The Permian granitic rocks are classic high-K, I-type granite. They have high silica and alkali contents, low MgO, TFe_2O_3, CaO, and transition-element contents, positive Th, Zr, and Hf anomalies, and negative Ba, Nb, Ta, P, and Ti anomalies in a primitive mantle-normalized diagram. These different characteristics indicate that the primary magma of these rocks originated from the partial melting of the continental crust, and may have been produced by the chemical differentiation of arc-derived magma [73,74]. The low Cao, Fe_2O_3, and MgO contents suggest that the source rock with this granitic component was likely formed under partial melting low-pressure conditions and that its source depths were relatively shallow. The negative anomalies of Nb were caused by the residual of rutile in the melt, since rutile is the main carrier mineral of Nb [75]. Therefore, the obvious depletions of Nb indicate residual rutile in the magma source of the Middle Permian monzogranite. Plagioclase, as the main carrier mineral of Ba, Sr, and Eu, becomes a residual mineral in the magma source in the event of negative anomalies in these elements. The negative Ba, Sr, and Eu anomalies of the granite sample indicate that plagioclase was retained in the residue of the source, or fractionated during magma evolution [76]. In conclusion, these Permian-age high-K, I-type granites were formed by partial melting of a lower crustal source under relatively low-pressure conditions.

5.3. Tectonic Implications and Geological Significance

5.3.1. Tectonic Setting

Tectonic Setting of the Middle Permian Monzogranite

In recent models, some scholars hold that the PAO closed in the Early Permian based on a late Early Permian-Middle Permian alkaline-peralkaline intrusion (276–259 Ma) distributed on the northern margin of the NCC, which indicates a post-collision environment in the Middle Permian [10,21,31]. All these intrusions studied by scholars are in the Jining area in the west section of the NCC's northern margin. However, the characteristics of the rock assemblages in the Middle Permian in the Changchun-Yanji area of the eastern section of the northern margin of the NCC show an active continental margin [74], while the widespread diorite, tonalite, and granodiorite indicate that the active continental marginal environment lasted until the Late Permian [38,77]. Therefore, the eastern section of the NCC's northern margin was still under the subduction background of the PAO in the Middle Permian [77]. In this case, then, what is the tectonic background of the Chifeng area in the central of the north margin of the NCC during the Middle Permian?

The Middle Permian granitic magma covers a large area in the Chifeng and is mainly dominated by monzogranite. Geochemical characteristics show that the monzogranite is the I-type granite originating from the lower crust. In the Y-Nb diagram, all samples fall into the volcanic arc and syn-collision area (Figure 10a). However, they fall into the transitional range between the volcanic arc and syn-collision and deviate to the syn-collision area in the Yb + Ta vs. Rb diagram (Figure 10b). In the R1-R2 structural environment discrimination diagram, they are in the group of syn-collision granite (Figure 11). Compared to the tectonic environment discriminant ratio of the orogenic granite proposed by Maniar and Piccoli (1989) [51], the monzogranite has characteristics like continental collision granite (CCG). Therefore, the Middle Permian monzogranite in the Chifeng area formed in a syn-collision environment.

Tectonic Setting of Late Permian Granite

Previous studies have shown that the Late Permian-Triassic magmatic rocks on the northern margin of the NCC exhibit post-collision/post-orogeny magmatism in terms of rock assemblage, mineral composition, high-potassium and calc-alkaline-based geochemical characteristics, magmatic evolution and isotope composition [8,28,29,37,53]. In the

R1-R2 diagram (Figure 11), all the Late Permian granites fall within the range of post-orogenic area, suggesting that the granite in the study area is related to the post-orogenic extension environment.
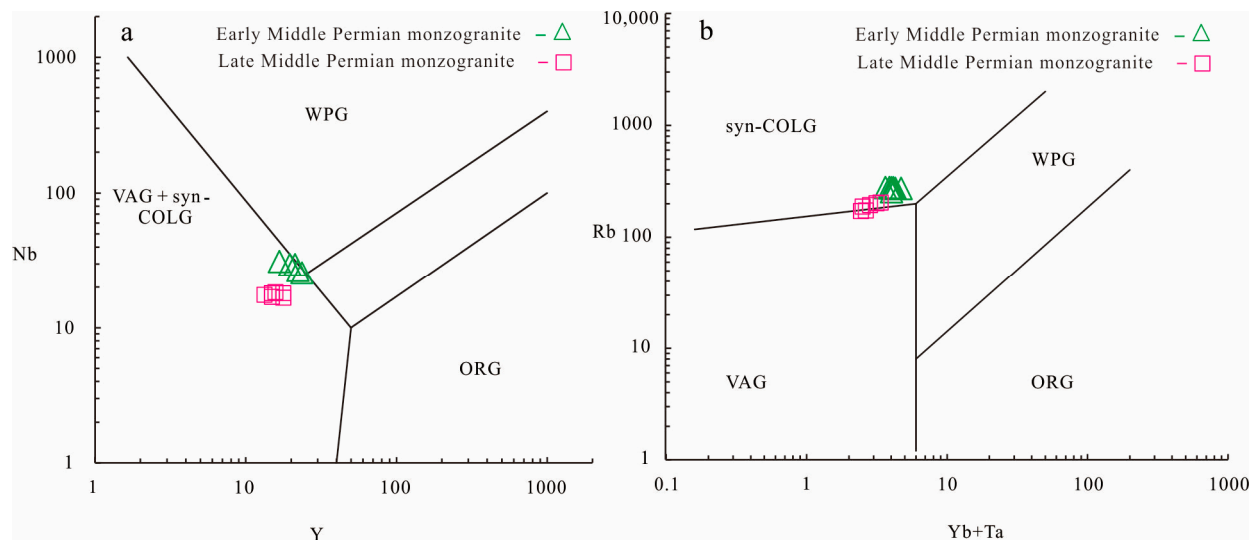

Figure 10. (**a**) Y versus Nb; (**b**) Yb + Ta versus Rb diagrams of the Middle Permian granites in Chifeng area (after [78]). The fields are ORG—oceanic ridge granites; syn-COLG—syn-collisional granites; VAG—volcanic arc granites; WPG—within-plate granites.
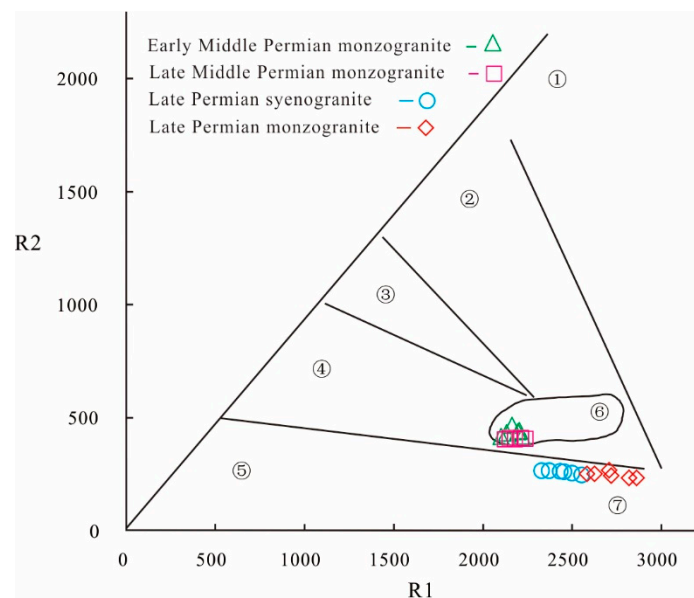

Figure 11. Diagram of R2 versus R1 for the Middle-Late Permian granites in the Chifeng area. ①—plagiogranite; ②—active continental margin granite; ③—collisional–orogenic granite; ④—late orogenic granite; ⑤—unorogenic A-type granite; ⑥—collisional granite (S-type); ⑦—post-orogenic granite (after [79]).

The granites that formed in the Chifeng area in the Late Permian and Early Triassic were of I- and A-type. Combined with the available data [8,15,40,53], these granites represent the acidic unit (256–248 Ma).The ophiolite formed from 256 to 246 Ma represents coeval basic members [7,33,35,36]. "Bimodal volcanic rocks" appeared between the northern margin of the NCC and XMOB in the Late Permian-Early Triassic. Previous studies have shown that bimodal volcanic rocks can be formed under the following extensional environments: continental rift, oceanic island extensional, plate margin extensional, post-orogenic extensional, oceanic island arc, mature island arc, and initial back-arc

basin [80,81]. The Late Permian granitic rocks in the Chifeng area are dominated by middle-high potassium calc-alkaline I- and A-type granite, indicating a post-orogenic extensional environment [57,82–86].

The Late Permian granite is characterized by the enrichment of light rare-earth elements and large ion lithophile elements (LILEs), and depletion of high field-strength elements (HFSEs) and elements such as Nb, Ti, and P, showing the characteristics of the granite in the post-collision evolutionary stage of continental orogenic belts. The tectonic environment discriminant map (Figure 12a–c) shows that all granites fall in the range of post-collision granite. In the Y + Nb-Rb and Yb + Ta-Rb diagrams, all the samples fall in the post-collision range, too (Figure 12d,e).
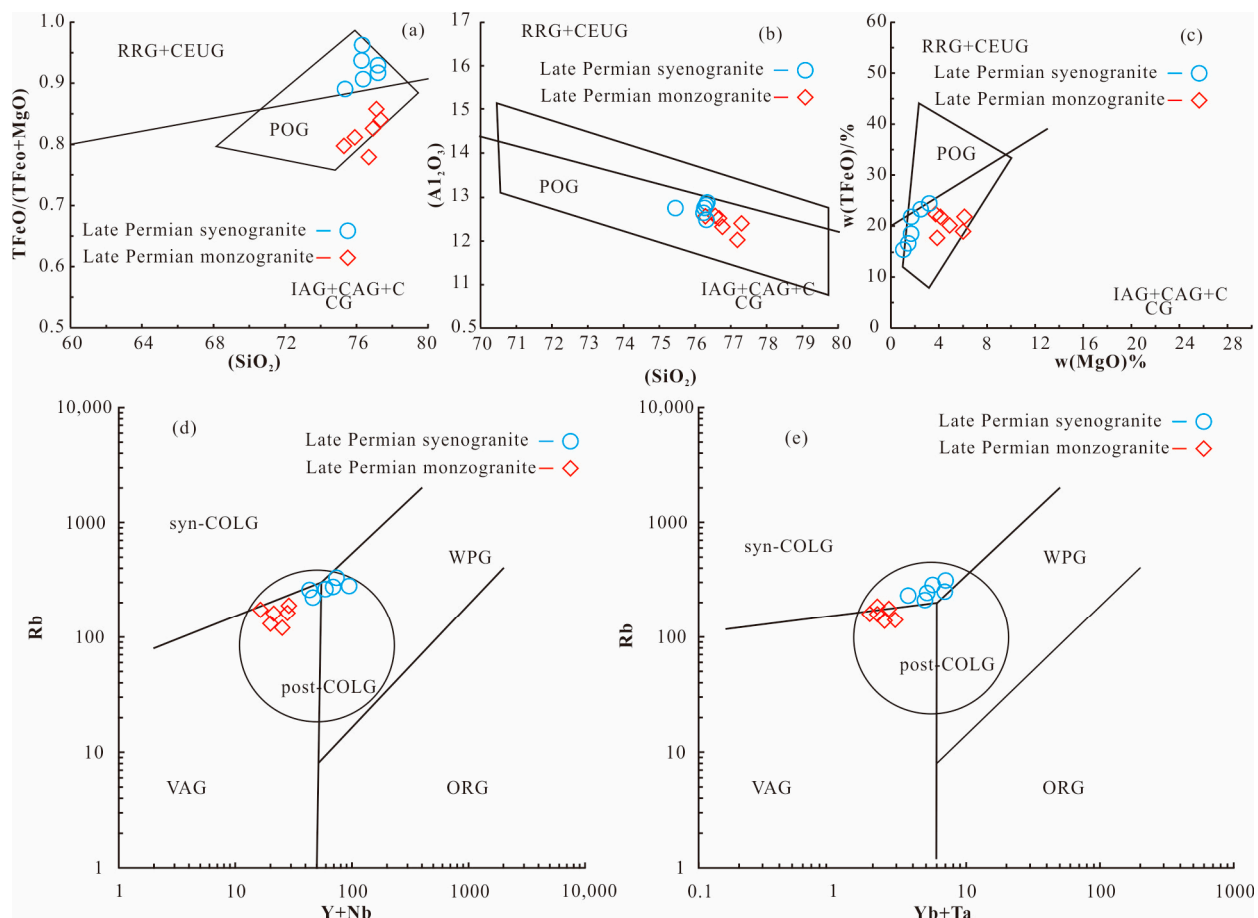

Figure 12. Identification diagram of tectonic setting for the Late Permian granites in the Chifeng area. (**a**) SiO_2 (wt%) versus $TFeO/(TFeO + MgO)$; (**b**) SiO_2 (wt%) versus Al_2O_2 (wt%); (**c**) MgO (wt%) versus TFeO (wt%), IAG—island arc granite; CAG—continental arc granite; CCG—continental collision granite; POG—post-orogenic granite; RRG—rift related granite; CEUG—continental epeirogenic uplift granite (after [51]). (**d**) Yb + Nb versus Rb, (**e**) Yb + Ta versus Rb (after [78]), VAG—volcanic arc granites; syn-COLG—syn-collisional granites; WPG—within-plate granites; ORG—oceanic ridge granites; post-COLG—post-collisional granites.

The post-collisional, which is usually considered to begin after the closure of the main ocean, is a complex period when large-scale horizontal block movement still occurred along the giant shear zone [64]. Most post-collision granites in orogenic belts are dominated by medium-high potassium calc-alkaline I-type granite, along with some S-type and A-type granites [87]. The appearance of various types of rock assemblages shows the complexity and diversity of post-collision magmatism [37,87]. In a post collision environment, the pressure decreases under the action of extension, which facilitates rock melting. The extensional environment leads to lithospheric crust thinning and mantle-derived magma

underplating. Sufficient heat then further drives the crust's partial melting, leading to the formation of many acidic rocks. Consequently, the appearance of these post-collision intermediate-acid igneous rocks may represent a transition environment from continental convergence to extension [64,88].

The following dynamic mechanisms may result in post-collision or post-orogenic magmatism: mantle convective thinning, gravity collapse, slab fragmentation, and delamination. As previously mentioned, the Late Permian-Early Triassic intrusive rocks with post-orogenic characteristics constitute a long and narrow magmatic rock belt, which spreads along both sides of the deep fault zone in the middle section of the northern margin of the NCC. The distribution pattern of Late Permian granites in the study area indicates that they were emplaced in an extensional environment caused by the slab breaking off after final closure of the PAO between the XMOB and NCC [8,89].

5.3.2. Permian Tectonic-Magmatic Evolution in the Chifeng Area

The chronological results show three phases of tectonic-magmatism in the Chifeng area during the Permian. The rock assemblage, geochemical characteristics, genesis, and tectonic setting of the granite from each phase are discussed here. Then, combined with previous research results, the Permian tectonic-magmatic evolution model is constructed (Figure 13), the specific dynamic process of which is as follows.
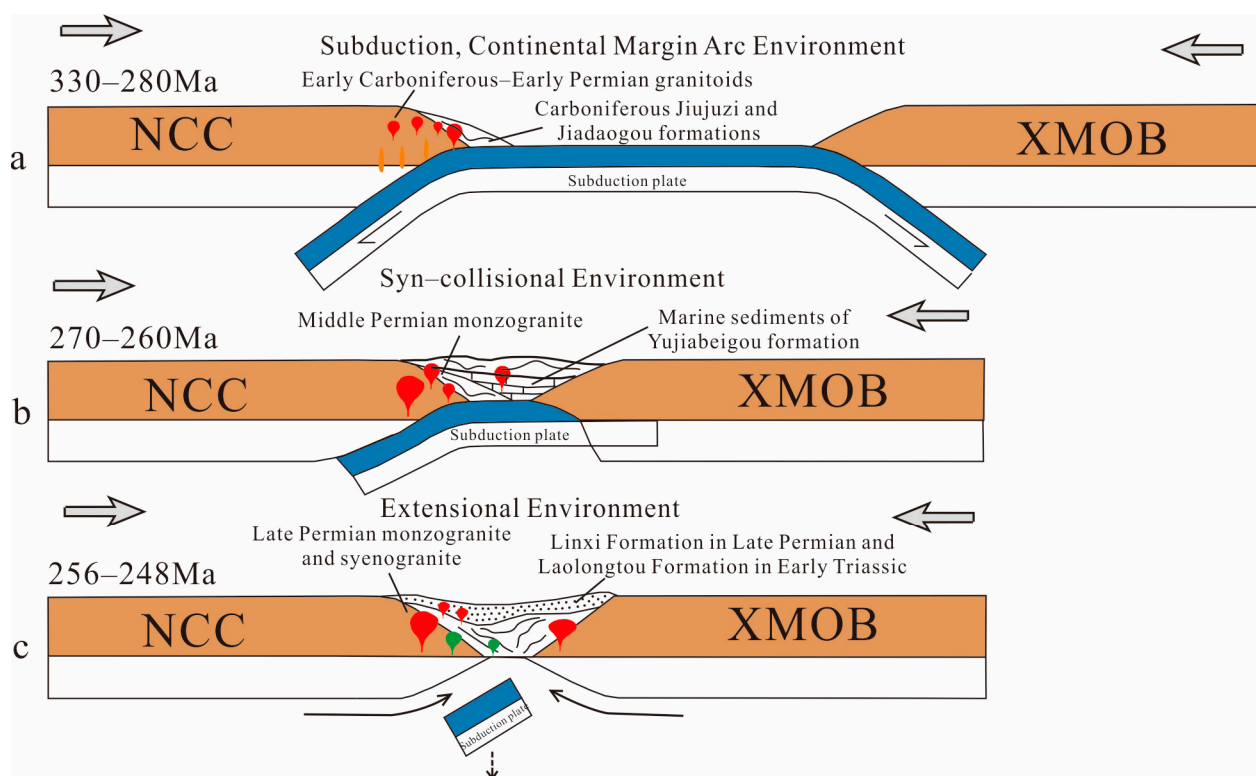

Figure 13. A tectonic evolution model from Carboniferous to Permian in the north margin of the NCC in the Chifeng-Aohan area. NCC, North China Craton; XMOB, Xing'an-Mongolian Orogenic Belt. (**a**): Subduction, Continental Margin Arc Environment; (**b**): Syn–collisional Environment; (**c**): Extensional Environment.

Early Permian–Active Continental Marginal Environment

The Early Permian granite in the Chifeng area formed in an active continental margin environment against the background of the PAO's southward subduction. The coeval volcanic rocks of the Permian Elitu Formation are also products of the subduction environment [22].

Regionally, the PAO began to subduct southward from the late Early Carboniferous, and magmatic rocks from the late Early Carboniferous to Middle Permian showed charac-

teristics of active continental margins in terms of distribution, rock assemblages, mineral compositions, geochemical characteristics, and isotopes, also known as an Andean active continental marginal arc [12,21,25]. The results of the SHRIMP U-Pb ages and geochemistry of several granite intrusive rocks in the northern margin of the NCC show that the granite has the characteristics of calc-alkaline and subduction-related I-type granite, with an emplacement age of 300–320 Ma. This indicates that there was an Andean continental arc in the NCC's northern margin, and that the PAO still existed in the Late Carboniferous-Early Permian, then eventually closed after 290 Ma [25]. Continuous Late Carboniferous-Early Permian (324–274 Ma) rock assemblages were identified on the northern margin of the NCC, including hornblende gabbro, diorite, quartz diorite, granodiorite, and granite. According to the geochemical characteristics of this group of intrusions, it is believed that the continental arc in the northern margin of the NCC lasted at least 50 Ma [90]. By studying the Early Permian granite in Xilinhot, Li et al. (2018) also confirmed that the northern margin of the NCC was in a continental marginal arc environment from the Late Carboniferous to the end of the Early Permian [22]. By studying the granite in Siziwang Banner, Wang (2014) proposed that the Early Permian quartz diorite formed in a continental marginal arc environment [10]. Li et al. (2018) also held that the Early Permian monzogranite and syenogranite in the western Chifeng area formed in a continental marginal arc environment [22].

From the above studies, the middle section of the northern margin of the NCC was under the tectonic environment of the active continental margin, due to southward subduction of the PAO during the Early Carboniferous-Early Permian (Figure 13a). As a result, Andean-type active continental margin calc-alkaline rock assemblages of west-east trending formed along the northern margin of the NCC. Based on previous data, the existence of the Early Carboniferous-Early Permian intrusive rocks (330–280 Ma) with high-potassium and calc-alkaline characteristics related to subduction implies that the subduction of the PAO lasted for at least 50 Ma [10,13,19,22,54].

The evidence of magmatic events indicates a magmatic arc lasting about 80 Ma in the Jining-Chifeng area in the middle section of the northern margin of the NCC during the Early Carboniferous-Early Permian (330–280 Ma) (Figure 13a). The entire northern margin of the NCC was likely in an active continental margin environment under the subduction, indicating that the PAO was not closed at this time.

Middle Permian-Continent-Continent Collision Environment

Geochemical characteristics show that the Middle Permian granite in the study area is monzogranite formed in a syn-collisional environment, indicating that the XMOB collided with the NCC at this time (Figure 13b). Collisional granite with an age of 230–250 Ma was identified in Sonid Left Banner, thus indicating that the PAO closed between 310 and 230 Ma [9,41]; thus, the collision between the XMOB and the NCC lasted from the Middle Permian to the Middle-Late Triassic. Li et al. (2007) discovered granite with SHRIMP U-Pb ages of 229 and 237 Ma and considered it to be S-type granite formed by the crystallization of younger remelted crust. The geochemical characteristics show that the Shuangjingzi intrusions were like syn-collisional granite, implying they likely emplaced in the late-collisional orogenic period. It was thus concluded that the XMOB and NCC collided along the Xar Moron suture zone beginning at about 270 Ma, and ending at 230 Ma [31].

During the early Middle Permian, the plant fossils in the Yujiabeigou Formation (the zircon age of crystalline tuff of which was 270 Ma) all belong to Cathaysian flora, and there was no mixing growth phenomenon, indicating the study area was a Cathaysian flora distribution area. At that time, the Solonker-Xar Moron-Changchun-Yanji suture zone was not yet closed [91], and the PAO developed into an intercontinental residual ocean basin. Subsequently, the oceanic crust was subducted, and continent-continent collision occurred, in turn forming multiple Middle Permian syn-collisional granitic intrusions. The gray-black slate and shale of the Linxi Formation from the Late Permian distributed in the southern margin of Inner Mongolia are rich in freshwater bivalves, leaf limbs, and plant fossils [39].

The Linxi Formation, which has marine sediments at the bottom and delta-lacustrine-delta continental deposits in the middle-upper part, indicates that two large plates had collided and collaged together, then jointly assimilated the deposition during the Late Permian [14]. The above evidence shows that the northern margin of the NCC was in a co-collisional environment, and that the monzogranite formed in the Chifeng area.

During the Middle Permian, the Jining area in the western section of the northern margin of the NCC was in a post-collisional environment [10,21,31], yet the Yanbian area in the eastern section was in an active continental margin environment [14,74]. The study area covered in this paper was between these two areas; thus, in the Middle Permian, it was also in a co-collisional environment. This proves that the PAO closed in a "scissor closure" mode from west to east.

Late Permian-Early Triassic-PAO Final Closure and Subduction Slab Break-off

The granite of the Late Permian-Early Triassic consisted of A- and I-type granite, and it formed in a post-collisional extensional environment in response to slab fragmentation after the collisional orogeny between the XMOB and the NCC (Figure 13c).

Today, there is much evidence to support the conclusion that the PAO was closed from the Late Permian to the Early Triassic. The build-up types, biota, and tectonic activities on both sides of the Xar Moron fault were obviously different during the Carboniferous-Permian. The paleobiogeographical flora were in disarray until the Middle or Late Permian [92]. Moreover, the Linxi Formation from the Late Permian and the Xingfuzhilu Formation from the Early Triassic were in conformity contact, indicating that the study area was in the same tectonic environment from the Late Permian to the Early Triassic [39]. There were continental deposits and terrestrial flora and fauna fossils in the Late Permian [39], thus indicating that the two major plates had collided and assimilated sedimentation together, resulting in the formation of the Linxi Formation [14]. According to the age of the radiolarian in the siliceous rocks of the Xar Moron, the final mixed accumulation time of the ophiolite belt was proposed to be the Middle-Late Permian [10]. Both the biological extinction event and paleomagnetic evidence indicated that the PAO closed at the end of the Late Permian [24].

There were large quantities of intrusive rocks with continental margin arc magmatic character on the northern margin of the NCC, and the emplacement age ranged from 358 to 260 Ma [21,37,42,93]. The appearance of the post-collisional A-type granite and the bimodal volcanic rocks and the emplacement of the coeval ophiolite also indicated that the PAO completely disappeared during the Permian-Early Triassic, and finally closed along the Xar Moron Suture Zone [7,8,25,28,29,94].

In summary, immediately after the Middle Permian continental collisional orogeny, the subducted slabs remaining in the lithospheric mantle experienced eclogite facies metamorphism and fragmented under the influence of gravity from the Late Permian to Early Triassic (Figure 13c). After the collision between the XMOB and the NCC, the Chifeng area was in an extensional environment. The crust underwent partial melting in response to the underplating of mantle-derived magma, the upwelling of deep asthenospheric mantle materials, increasing heat, and decreasing pressure. As a result, the post-collisional A-type granite of west–east trending, bimodal volcanic rock, and ophiolite formed during the Late Permian-Early Triassic. The lacustrine Linxi Formation had abundant freshwater bivalves and gray-black slate and shale containing leaf limbs and plant fossils [14]. In addition, the paleobiogeographical divisions disappeared. All of these indicate that the PAO finally closed along the Solonker-Xar Moron-Changchun-Yanji Suture (SXCYS) during the Late Permian-Early Triassic, at which time the ocean basin completely disappeared [8,28,29].

6. Conclusions

In this study, on the Permian granitic rocks of the northern margin of the NCC, the following conclusions were obtained:

(1)　According to the zircon U-Pb dating results, three events of Permian granitic magmatism were identified in the Chifeng area: (1) a suite of syenogranites and monzogranites dated at ca. 294–284 Ma (Cisuralian); (2) a suite of monzogranites dated at ca. 269–260 Ma (Guadalupian); and (3) a suite of monzogranites and syenogranites dated at ca. 256–254 Ma (Lopingian).

(2)　The two events related to the Middle Permian monzogranite represent I-type granite with Al-saturated, Si- and K-rich, negative Eu anomaly; enrichment of LILEs (Rb, Th, K, and La); and negative Sr, P, and Ti anomalies. The Late Permian syenogranite is rich in Si and K and poor in Al, classified as I-type granite with moderately negative Eu anomalies; enrichment of LILEs (Rb, Th, K, La, and Ce); minor enrichment in HFSEs (Nd, Zr, and Hf); and negative anomalies of Ba, P, Ti, and Sr. These Permian high-K I-type granites were formed by partial melting of the lower crustal source under relatively low-pressure conditions. The Late Permian monzogranite is A-type granite, displaying a "V" shape of rare-earth elements, with strongly negative Eu anomalies; enrichment of LILES (Rb, Th, U, and K); negative anomalies of Ba, P, and Ti; and obvious Sr negative anomalies, formed in a low-pressure environment caused by tension.

(3)　The Permian tectono-magmatic evolution of the PAO can be divided into three events: (1) Early Permian granite formed in the setting of the PAO subducting to the NCC; (2) Middle Permian granite formed during the collision of the XMOB and the NCC; and (3) Late Permian-Early Triassic granite formed in an extensional setting induced by the slab breaking off after the collision between the XMOB and the NCC, responsible for the closing of the PAO.

Author Contributions: Conceptualization, J.C.; formal analysis, J.C., D.T., B.L. and Y.S.; investigation, D.T., B.L., Y.S., Z.G., Y.T., W.L., C.Z. and Y.W.; writing—original draft preparation, J.C., B.L. and Y.S.; writing—review and editing, J.C., B.L. and Y.S.; projection administration, Y.W. All authors have read and agreed to the published version of the manuscript.

Data Availability Statement: The authors confirm that the data generated or analyzed during this study are provided in full within the published article.

Conflicts of Interest: Authors Zhonghui Gao, Yi Tian, and Weiwei Li were employed by the company Institute of Geology and Mineral Resources of Liaoning Co., Ltd. The remaining authors declare that the research was conducted in the absence of any commercial or financial relationships that could be construed as a potential conflict of interest.

References

1.　Sengör, A.M.C.; Natal'in, B.A. Paleotectonics of Asia: Fragments of a synthesis. In *The Tectonic Evolution of Asia*; Yin, A., Harrison, T.M., Eds.; Cambrige University Press: Cambridge, UK, 1996; pp. 486–641.

2.　Sengör, A.M.C.; Natal'in, B.A.; Burtman, V.S. Evolution of the altaid tectonic collage and Palaeozoic crustal growth in Eurasia. *Nature* **1993**, *364*, 299–307. [CrossRef]

3. Jahn, B.M. The Central Asian Orogenic Belt and growth of the continental crust in the Phanerozoic. *Geol. Soc. Lond. Spec. Publ.* **2004**, *226*, 73–100. [CrossRef]

4. Li, J.Y. Permian geodynamic setting of northeast China and adjacent regions: Closure of the Paleo-Asian Ocean and subduction of the Paleo-Pacific Plate. *J. Asian Earth Sci.* **2006**, *26*, 207–224. [CrossRef]

5. Wu, F.Y.; Sun, D.Y.; Ge, W.C.; Zhang, Y.B.; Grant, M.L.; Wilde, S.A.; Jahn, B.M. Geochronology of the Phanerozoic granitoids in Northeastern China. *J. Asian Earth Sci.* **2011**, *41*, 1–30. [CrossRef]

6. Wu, F.Y.; Sun, D.Y.; Li, H.M.; Jahn, B.M.; Wilde, S.A. A-type granites in Northeastern China: Age and geochemical constraints on their petrogenesis. *Chem. Geol.* **2002**, *187*, 143–173. [CrossRef]

7. Song, S.G.; Wang, M.M.; Xu, X.; Wang, C.; Niu, Y.L.; Allen, M.B.; Su, L. Ophiolites in the Xing'an-Inner Mongolia accretionary belt of the CAOB: Implications for two cycles of seafloor spreading and accretionary orogenic events. *Tectonics* **2015**, *34*, 2221–2248. [CrossRef]

8. Chen, J.S.; Tian, D.X.; Yang, H.; Li, W.W.; Liu, M.; Li, B.; Yang, F.; Li, W.; Wu, Z. Triassic granitic magmatism at the northern margin of the North China Craton: Implications of geochronology and geochemistry for the tectonic evolution of the Central Asian Orogenic Belt. *Acta Geol. Sin.* **2019**, *93*, 1325–1353. [CrossRef]

9. Chen, B.; Jahn, B.M.; Tian, W. Evolution of the Solonker Suture Zone: Constraints from zircon U-Pb ages, Hf isotopic ratios and whole-rock Nd-Sr isotope compositions of subduction- and collision-related magmas and forearc sediments. *J. Asian Earth Sci.* **2009**, *34*, 245–257. [CrossRef]

10. Wang, W.Q. Late Paleozoic Tectonic Evolution of the Central-Northern Margin of the North China Craton: Constraints from Zircon U-Pb Ages and Geochemistry of Igneous Rocks in Ondor Sum-Jining Area. Ph.D. Thesis, Jilin University, Changchun, China, 2014; pp. 1–169. (In Chinese with English Abstract)

11. Chen, J.S.; Liu, Z.H.; Liu, Y.J.; Feng, Z.Q.; Zhang, L.D.; Wang, Y. Recent progress in the tectonic evolution of the eastern segment of Central Asia Orogenic Belt. *Acta Petrol. Sin.* **2022**, *38*, 2175–2180. (In Chinese with English Abstract)

12. Xiao, W.J.; Windley, B.F.; Hao, J.; Zhai, M.G. Accretion leading to collision and the Permian Solonker Suture, Inner Mongolia, China: Termination of the Central Asian Orogenic Belt. *Tectonics* **2003**, *22*, 1069–1090. [CrossRef]

13. Zhang, S.H.; Zhao, Y.; Song, B.; Hu, J.M.; Liu, S.W.; Yang, Y.H.; Chen, F.K.; Liu, X.M.; Liu, J. Contrasting Late Carboniferous and Late Permian-Middle Triassic intrusive suites from the northern margin of the North China Craton: Geochronology, petrogenesis, and tectonic implications. *Geol. Soc. Am. Bull.* **2009**, *121*, 181–200. [CrossRef]

14. Zhao, Y.L.; Li, W.M.; Wen, Q.B.; Liang, T.Y.; Feng, Z.Q.; Zhou, J.P.; Shen, L. Late Paleozoic tectonic framework of eastern Inner Mongolia: Evidence from the detrital zircon U-Pb ages of the Mid-Late Permian to Early Triassic sandstones. *Acta Petrol. Sin.* **2016**, *32*, 2807–2822. (In Chinese with English Abstract)

15. Liu, Y.; Xi, A.H.; Ge, Y.H.; Tang, X.Y.; Xu, B.W.; Wang, M.Z.; Ma, Y.J. LA-ICP-MS zircon U-Pb ages and petrogenesis of granodiorite in Mengguyingzi, Chifeng, Inner Mongolia. *Geol. Bull. China* **2015**, *34*, 437–446. (In Chinese with English Abstract)

16. Liu, Y.J.; Li, W.M.; Feng, Z.Q.; Wen, Q.B.; Neubauer, F.; Liang, C.Y. A review of the Paleozoic tectonics in the eastern part of Central Asian Orogenic Belt. *Gondwana Res.* **2017**, *43*, 123–148. [CrossRef]

17. Tang, K.D. Tectonic development of Paleozoic fold belts at the northern margin of the Sino-Korean Craton. *Tectonics* **1990**, *9*, 249–260. [CrossRef]

18. Tang, K.D.; Ju, N.; Zhang, D.Q.; Zhang, G.B.; Feng, Y.; Sun, J.G. Implication of the tectonic eveolution of Paleo-Asian Ocean. *Geol. Resour.* **2022**, *31*, 246–259. (In Chinese with English Abstract)

19. Zhang, S.H.; Zhao, Y.; Davis, G.A.; Ye, H.; Wu, F. Temporal and spatial variations of Mesozoic magmatism and deformation in the North China Craton: Implications for lithospheric thinning and decratonization. *Earth-Sci. Rev.* **2014**, *131*, 49–87. [CrossRef]

20. Zhao, P.; Jahn, B.; Xu, B.; Liao, W.; Wang, Y. Geochemistry, geochronology and zircon Hf isotopic study of peralkaline-alkaline intrusions along the northern margin of the North China Craton and its tectonic implication for the southeastern Central Asian Orogenic Belt. *Lithos* **2016**, *261*, 92–108. [CrossRef]

21. Zhang, S.H.; Zhao, Y.; Song, B.; Yang, Z.Y.; Hu, J.M.; Wu, H. Carboniferous granitic plutons from the northern margin of the North China Block: Implications for a Late Palaeozoic active continental margin. *J. Geol. Soc. Lond.* **2007**, *164*, 451–463. [CrossRef]

22. Li, B.; Chen, J.S.; Liu, M.; Yang, F.; Li, W.; Wu, Z.; Chen, M.H.; Wu, C.S. LA-ICP-MS zircon U-Pb geochronology and geochemical characteristics of the Early Permian granite in Chifeng area, Inner Mongolia. *Geol. Bull. China* **2018**, *37*, 1671–1681. (In Chinese with English Abstract)

23. Wang, Q.; Liu, X.Y. Paleoplate tectonics between Cathasia and Angaraland in Inner Mongolia of China. *Tectonics* **1986**, *5*, 1073–1088. [CrossRef]

24. Li, P.W.; Gao, R.; Guan, Y.; Li, Q.S. The closed times of the Paleo-Asian Ocean and the Paleo-Tethys Ocean: Implication for the tectonic cause of the End-Permian mass extinction. *J. Jilin Univ.* **2009**, *39*, 521–527. (In Chinese with English Abstract)

25. Zhang, S.H.; Zhao, Y.; Song, B. Hornblende thermobarometry of the Carboniferous granitoids from the Inner Mongolia Paleo-Uplift: Implications for the geotectonic evolution of the northern margin of North China Block. *Mineral. Petrol.* **2006**, *87*, 123–141. [CrossRef]

26. Windley, B.F.; Alexeiev, D.; Xiao, W.J.; Kroener, A.; Badarch, G. Tectonic models for accretion of the Central Asian Orogenic Belt. *J. Geol. Soc. Lond.* **2007**, *164*, 31–48. [CrossRef]

27. Guan, Q.B.; Liu, Z.H.; Liu, Y.J.; Liu, J.; Wang, S.J.; Tian, Y. Geochemistry and zircon U–Pb geochronology of mafic rocks in the Kaiyuan tectonic mélange of northern Liaoning Province, NE China: Constraints on the tectonic evolution of the Paleo-Asian Ocean. *Geol. J.* **2019**, *54*, 656–678. [CrossRef]

28. Shi, S.S.; Shi, Y.; Zhang, C.; Shi, J.M.; Jiang, S. Geochronology and geochemistry of the Triassic intrusive rocks in the Faku area, northern Liaoning, China: Constraints on the evolution of the Palaeo-Asian Ocean. *Geol. J.* **2022**, *57*, 1658–1681. [CrossRef]

29. Chen, J.S.; Li, W.W.; Shi, Y.; Li, B.; Zhao, C.Q.; Zhang, L.D. Evolution of the eastern segment of the the northern margin of the North China Craton in the Triassic: Evidence from the geochronology and geochemistry of magmatic rocks in Kaiyuan area, North Liaonign. *Acta Petrol. Sin.* **2022**, *38*, 2216–2248. (In Chinese with English Abstract)

30. Wang, Y.J. A review of the study of the Paleozoic radiation of the Paleozoic in China. *Acta Micropalaeontological Sin.* **2001**, *18*, 313–320. (In Chinese with English Abstract) [CrossRef]

31. Li, J.Y.; Gao, L.M.; Sun, G.H.; Li, Y.P.; Wang, Y.B. Shuangjingzi Middle Triassic syn-collisional crust-derived granite in the East Inner Mongolia and its constraint on the timing of collision between Siberian and Sino-Korean Paleo-plates. *Acta Petrol. Sin.* **2007**, *23*, 565–582. (In Chinese with English Abstract)

32. Tian, S.G.; Li, Z.S.; Zhang, Y.S.; Gong, Y.X.; Zhai, D.X.; Wang, M. Late Carboniferous-Permian tectono-geographical conditions and development in eastern Inner Mengolia and adjacent areas. *Acta Geol. Sin.* **2016**, *90*, 688–707. (In Chinese with English Abstract)

33. Miao, L.C.; Fan, W.M.; Liu, D.Y.; Zhang, F.Q.; Shi, Y.R.; Guo, F. Geochronology and geochemistry of the Hegenshan ophiolitic complex: Implications for late-stage tectonic evolution of the Inner Mongolia-Daxinganling Orogenic Belt, China. *J. Asian Earth Sci.* **2008**, *32*, 348–370. [CrossRef]

34. Robinson, P.T.; Zhou, M.F.; Hu, X.F.; Reynolds, P.; Bai, W.J.; Yang, J.S. Geochemical constraints on the oringin of the Hegenshan ophiolite, Inner Mongolia, China. *J. Asian Earth Sci.* **1999**, *17*, 423–442. [CrossRef]

35. Jian, P.; Liu, D.Y.; KröNer, A.; Windley, B.F.; Shi, Y.R.; Zhang, W.; Zhang, F.Q.; Miao, L.C.; Zhang, L.Q.; Tomurhuu, D. Evolution of a Permian intraoceanic arc-trench system in the Solonker Suture Zone, Central Asian Orogenic Belt, China and Mongolia. *Lithos* **2010**, *118*, 169–190. [CrossRef]

36. Chu, H.; Zhang, J.R.; Wei, C.J.; Wang, H.C.; Ren, Y.W. A new interpretation of the tectonic setting and age of meta-basic volcanics in the Ondor Sum Group, Inner Mongolia, China. *Sci. Bull.* **2013**, *58*, 3580–3587. [CrossRef]

37. Zhang, S.H.; Zhao, Y.; Liu, J.M.; Hu, J.M.; Song, B.; Liu, J.; Wu, H. Geochronology, geochemistry and tectonic setting of the Late Paleozoic-Early Mesozoic magmatism in the northern margin of the North China Block: A preliminary review. *Acta Petrol. Et Mineral.* **2010**, *29*, 824–842. (In Chinese with English Abstract)

38. Zhang, Y.B.; Wu, F.Y.; Wilde, S.A.; Zhai, M.G.; Lu, X.P.; Sun, D.Y. Zircon U-Pb ages and tectonic implications of "Early Paleozoic" granitoids at Yanbian, Jilin Province, Northeast China. *Isl. Arc* **2004**, *13*, 484–505. [CrossRef]

39. Zhang, S.H.; Zhao, Y.; Ye, H.; Hou, K.J.; Li, C.F. Early Mesozoic alkaline complexes in the northern North China Craton: Implications for cratonic lithospheric destruction. *Lithos* **2012**, *155*, 1–18. [CrossRef]

40. Duan, P.X.; Li, C.M.; Liu, C.; Deng, J.F.; Zhao, G.C. Geochronology and geochemistry of the granites from the Jinchanggouliang gold deposit area in the Inner Mongolia and its geological significance. *Acta Petrol. Sin.* **2014**, *30*, 3189–3202. (In Chinese with English Abstract)

41. Chen, B.; Jahn, B.M.; Wilde, S.A.; Xu, B. Two contrasting Paleozoic magmatic belts in northern Inner Mongolia, China: Petrogenesis and tectonic implications. *Tectonophysics* **2000**, *328*, 157–182. [CrossRef]

42. Chen, J.S.; Li, B.; Yang, H.; Liu, M.; Yang, F.; Li, W.; Wang, Y.; Cui, T.R. New zircon U-Pb age of granodiorite in Chifeng at the northern margin of North China Craton and constraints on plate tectonic evolution. *Acta Geol. Sin.* **2018**, *92*, 410–413. [CrossRef]

43. Wiedenbeck, M.; Allé, P.; Corfu, F.; Griffin, W.L.; Meier, M.; Oberli, F.; Quadt, A.; Roddick, J.C.; Spiegel, W. Three natural zircon standards for U-Th-Pb, Lu-Hf, trace element and REE analyses. *Geostand. Geoanalytical Res.* **1995**, *19*, 1–23. [CrossRef]

44. Black, L.P.; Kamo, S.L.; Allen, C.M.; Davis, D.W.; Aleinikoff, J.N.; Valley, J.W.; Mundil, R.; Campbell, I.H.; Korsch, R.J.; Williams, I.S.; et al. Improved $^{206}Pb/^{238}U$ microprobe geochronology by the monitoring of a trace-element-related matrix effect; SHRIMP, ID–TIMS, ELA–ICP–MS and oxygen isotope documentation for a series of zircon standards. *Chem. Geol.* **2004**, *205*, 115–140. [CrossRef]

45. Ludwig, K.R. User's manual for isoplot 3.0: A geochronological toolkit for microsoft excel. *Berkeley Geochronol. Cent. Spec. Publ.* **2003**, *4*, 1–70.

46. Andersen, T. Correction of common Lead in U-Pb analyses that do not report ^{204}Pb. *Chem. Geol.* **2002**, *192*, 59–79. [CrossRef]

47. Horstwood, M.S.A.; Košler, J.; Gehrels, G.; Jackson, S.E.; McLean, N.M.; Paton, C.; Pearson, N.J.; Sircombe, K.; Sylvester, P.; Vermeesch, P. Community-derived standards for LA-ICP-MS U-(Th-) Pb geochronology–Uncertainty propagation, age interpretation and data reporting. *Geostand. Geoanalytical Res.* **2016**, *40*, 311–332. [CrossRef]

48. Belousova, E.; Griffin, W.; O'Reilly, S.Y.; Fisher, N. Igneous zircon: Trace element composition as an indicator of source rock type. *Contrib. Mineral. Petrol.* **2002**, *143*, 602–622. [CrossRef]

49. Hoskin, P.W.O.; Ireland, T.R. Rare earth element chemistry of zircon and its use as a provenance indicator. *Geology* **2000**, *28*, 627–630. [CrossRef]

50. Peccerillo, A.; Taylor, S.R. Geochemistry of Eocene calc-alkaline volcanic rocks from the Kastamonu area, northern Turkey. *Contrib. Mineral. Petrol.* **1976**, *58*, 63–81. [CrossRef]

51. Maniar, P.D.; Piccoli, P.M. Tectonic discrimination of granitoids. *Geol. Soc. Am. Bull.* **1989**, *101*, 635–643. [CrossRef]

52. Sun, S.S.; McDonough, W.F. Chemical and isotopic systematics of oceanic basalts: Implications for mantle composition and processes. *Geol. Soc. Lond. Spec. Publ.* **1989**, *42*, 313–345. [CrossRef]

53. Shao, J.A.; Zhang, Z.; She, H.Q.; Liu, D.S. The discovery of Phanerozoic granulite in Chifeng area of North Craton and its implication. *Earth Sci. Front.* **2012**, *19*, 187–198. (In Chinese with English Abstract)

54. Jiang, S.H.; Liang, Q.L.; Nie, F.J.; Liu, Y.F. A preliminary study of zircon LAMC-ICP-MS U-Pb ages of the Shuangjingzi complex in Linxi, Inner Mongolia. *Geol. China* **2014**, *41*, 1108–1123. (In Chinese with English Abstract)

55. Xi, A.H.; Ma, Y.J.; Ge, Y.H.; Tang, X.Y.; Liu, S.; Xu, B.W.; Liu, Y. Multi-stage intrusive evidence and geological significance of Dayingzi granite in Chifeng, Eastern Inner Mongolia. *J. Jilin Univ.* **2015**, *45*, 791–803. (In Chinese with English Abstract)

56. Whalen, J.B.; Currie, K.L.; Chappell, B.W. A-type granites: Geochemical characteristics, discrimination and petrogenesis. *Contrib. Mineral. Petrol.* **1987**, *95*, 407–419. [CrossRef]

57. Zhang, Q.; Ran, A.; Li, C.D. A-type granite: What is the essence? *Acta Petrol. Mineral.* **2012**, *31*, 621–626. (In Chinese with English Abstract)

58. Chappell, B.W.; White, A.J. I- and S-type granites in the Lachlan Fold Belt. *Trans. R. Soc. Edinb. Earth Sci.* **1992**, *83*, 1–26.

59. Clemens, J.D.; Holloway, J.R.; White, A.J. Origin of A-type granites: Experimental constraints. *Am. Miner.* **1986**, *71*, 317–324.

60. Anderson, J.L. Proterozoic anorogenic granite plutonism of North America. *Mem. Geol. Soc. Am.* **1983**, *161*, 133–154.

61. Scaillet, B.; Macdonald, R. Phase relations of peralkaline silicic magmas and petrogenetic implications. *J. Petrol.* **2001**, *42*, 825–845. [CrossRef]

62. Scaillet, B.; Macdonald, R. Experimental constraints on the relationships between peralkaline rhyolites of the Kenya Rift Valley. *J. Petrol.* **2003**, *44*, 1867–1894. [CrossRef]

63. Roberts, M.P.; Clemens, J.D. Origin of high-potassium, calc-alkaline, I-type granitoids. *Geology* **1993**, *21*, 825–828. [CrossRef]

64. Liegeois, J.P.; Navez, J.; Hertogen, J.; Black, R. Contrasting origin of postcollisional high-K calc-alkaline and shoshonitic versus alkaline and peralkaline granitoids: The use of sliding normalization. *Lithos* **1998**, *45*, 1–28. [CrossRef]

65. DePaolo, D.J. Trace element and isotopic effects of combined wallrock assimilation and fractional crystallization. *Earth Planet. Sci. Lett.* **1981**, *53*, 189–202. [CrossRef]

66. Moghazi, A.M. Geochemistry and petrogenesis of a high-K calc-alkaline Dokhan Volcanic suite, South Safaga area, Egypt: The role of late Neoproterozoic crustal extension. *Precambrian Res.* **2003**, *125*, 161–178. [CrossRef]

67. Dickinson, W.R. Potash-depth (K-h) relations in continental-margin and intraoceanic magmatic arcs. *Geology* **1975**, *3*, 53–56. [CrossRef]

68. Yang, H.; Ge, W.C.; Zhao, G.C.; Dong, Y.; Xu, W.L.; Wang, Z.H.; Ji, Z.; Yu, J.J. Late Triassic intrusive complex in the Jidong region, Jiamusi-Khanka Block, NE China: Geochemistry, zircon U-Pb ages, Lu-Hf isotopes, and implications for magma mingling and mixing. *Lithos* **2015**, *224–225*, 143–159. [CrossRef]

69. Yang, J.H.; Wu, F.Y.; Chung, S.L.; Wilde, S.A.; Chu, M.F. A hybrid origin for the Yianshan A-type granite, northeast China: Geochemical and Sr-Nd-Hf isotopic evidence. *Lithos* **2006**, *89*, 89–106. [CrossRef]

70. Clemens, J.D.; Darbyshire, D.P.F.; Flinders, J. Sources of post-orogenic calcalkaline magmas: The Arrochar and Garabal Hill-Glen Fyne complexes, Scotland. *Lithos* **2009**, *112*, 524–542. [CrossRef]

71. Sisson, T.W.; Ratajeski, K.; Hankins, W.B.; Glazner, A.F. Voluminous granitic magmas from common basaltic sources. *Contrib. Mineral. Petrol.* **2005**, *148*, 635–661. [CrossRef]

72. Topuz, G.; Altherr, R.; Siebel, W.; Schwarz, W.H.; Zack, T.; Hasözbek, A.; Barth, M.; Satır, M.; Şen, C. Carboniferous high-potassium I-type granitoid magmatism in the Eastern Pontides: The Gümüşhane pluton (NE Turkey). *Lithos* **2010**, *116*, 92–110. [CrossRef]

73. Hofmann, A.W. Chemical differentiation of the Earth: The relationship between mantle, continental crust, and oceanic crust. *Earth Planet. Sci. Lett.* **1988**, *90*, 297–314. [CrossRef]

74. Yu, J.J.; Wang, F.; Xu, W.L.; Gao, F.H.; Tang, J. Late Permian tectonic evolution at the southeastern margin of the Songnen-Zhangguangcai Range Massif, NE China: Constraints from geochronology and geochemistry of granitoids. *Gondwana Res.* **2013**, *24*, 635–647. [CrossRef]

75. Xiong, X.L.; Adam, J.; Green, T.H. Rutile stability and rutile/melt HFSE partitioning during partial melting of hydrous basalt: Implications for TTG genesis. *Chem. Geol.* **2005**, *218*, 339–359. [CrossRef]

76. Springer, W.; Seck, H.A. Partial fusion of basic granulites at 5-15 kbar: Implications for the origin of TTG magmas. *Contrib. Mineral. Petrol.* **1997**, *127*, 30–45. [CrossRef]

77. Cao, H.H.; Xu, W.L.; Pei, F.P.; Zhang, X.Z. Permian tectonic evolution in southwestern Khanka massif: Evidence from zircon U-Pb chronology, Hf isotope and geochemistry of gabbro and diorite. *Acta Geol. Sin.* **2011**, *85*, 1390–1402.

78. Pearce, J.A. A user's guide to basalt discrimination diagrams. In *Trace Element Geochemistry of Volcanic Rocks: Applications for Massive Sulphide Exploration*; Wyman, D.A., Ed.; Geological Association of Canada, Short Course Notes: St. John's, NF, Canada, 1996; Volume 12, pp. 79–113.

79. Batchelor, R.A.; Bowden, P. Petrogenetic interpretation of granitoid rock series using multicationic parameters. *Chem. Geol.* **1985**, *48*, 43–55. [CrossRef]

80. Ikeda, Y.; Yuasa, M. Volcanism in Nascent backarc basins behind the Schichito ridge and adjacent areas in the Izu-Ogasawara Arc, NW Pacific: Evidence for mixing between E-type MORB and island arc magmas at the initiation of back-arc rifting. *Contrib. Mineral. Petrol.* **1989**, *101*, 377–393. [CrossRef]

81. Pin, C.; Paquette, J.L. A mantle-derived bimodal suite in the Hercynian belt: Nd isotope and trace element evidence for a subduction-related rift origin of the Late Devonian brevenne metavolcanics, Massif Central (France). *Contrib. Mineral. Petrol.* **1997**, *129*, 222–238. [CrossRef]

82. Hildreth, W.E.; Halliday, A.N.; Christiansen, R.L. Isotopic and chemical evidence concerning the genesis and contamination of basaltic and rhyolitic magma beneath the Yellowstone Plateau Volcanic Field. *J. Petrol.* **1991**, *32*, 63–138. [CrossRef]

83. Eby, G.N. Chemical subdivision of the A-type granitoids: Petrogenetic and tectonic implications. *Geology* **1992**, *20*, 641–644. [CrossRef]

84. Turner, S.; Sandiford, M.; Foden, J. Some geodynamic and compositional constraints on "postorogenic" magmatism. *Geology* **1992**, *20*, 931–934. [CrossRef]

85. Frost, C.D.; Frost, B.R.; Chamberlain, K.R.; Edwards, B.R. Petrogenesis of the 1.43 Ga Sherman batholith, SE Wyoming, USA: A reduced, rapakivi-type anorogenic granite. *J. Petrol.* **1999**, *40*, 1771–1802. [CrossRef]

86. Bonin, B. Do coeval mafic and felsic magmas in post-collisional to within-plate regimes necessarily imply two contrasting, mantle and crustal, sources? A review. *Lithos* **2004**, *78*, 1–24. [CrossRef]

87. Han, B.F. Diverse post-collisional granitoids and their tectonic setting discrimination. *Earth Sci. Front.* **2007**, *14*, 64–72. (In Chinese with English Abstract)

88. Barbarin, B. A review of the relationships between granitoid types, their origins and their geodynamic environments. *Lithos* **1999**, *46*, 605–626. [CrossRef]

89. Von Blanckenburg, F.; Davies, J.H. Slab breakoff: A model for syncollisional magmatism and tectonics in the Alps. *Tectonics* **1995**, *14*, 120–131. [CrossRef]

90. Zhang, S.H.; Zhao, Y.; Kroner, A.; Liu, X.M.; Xie, L.W.; Chen, F.K. Early Permian plutons from the northern North China Block: Constraints on continental arc evolution and convergent margin magmatism related to the Central Asian Orogenic Belt. *Int. J. Earth Sci.* **2009**, *98*, 1441–1467. [CrossRef]

91. Sun, Y.W.; Ding, H.S.; Liu, H.; Zhang, D.J.; Gong, F.H.; Zheng, Y.J. Fossil plants from the Guadalupian Yujiabeigou Formation in the north margin of North China Plate and their tectonic implications. *J. Jilin Univ.* **2016**, *46*, 1268–1283. (In Chinese with English Abstract)

92. Huang, B.H.; Ding, Q.H. The angara flora from Northern China. *Acta Geosci. Sin.* **1998**, *19*, 97–104. (In Chinese with English Abstract)

93. Shi, Y.; Shi, S.S.; Liu, Z.H.; Liu, J.; Ju, N.; You, H.X.; Zhang, Z.B.; Zhao, C.Q. Petrogenesis of the late Early Palaeozoic adakitic granitoids in the southern margin of the Songliao Basin, NE China: Implications for the subduction of the Palaeo-Asian Ocean. *Geol. J.* **2019**, *54*, 3821–3839. [CrossRef]

94. Miao, L.C.; Zhang, F.Q.; Fan, W.M.; Liu, D.Y. Phanerozoic evolution of the Inner Mongolia-Daxinganling Orogenic Belt in North China: Constraints from geochronology of ophiolites and associated formations. *Geol. Soc. Lond. Spec. Publ.* **2007**, *280*, 223–237. [CrossRef]